NUCLEIC ACID-DRIVEN QUANTUM DOT-BASED LATTICE FORMATIONS FOR BIOMEDICAL APPLICATIONS

by

Brandon Kyle Roark

A thesis submitted to the faculty of
The University of North Carolina at Charlotte
in partial fulfillment of the requirements
for the degree of Master of Science in
Chemistry

Charlotte

2017

Approved by:

_____
Dr. Kirill Afonin

_____
Dr. Marcus Jones

_____
Dr. Hansang Cho

_____
Dr. Jerry Troutman

ABSTRACT

BRANDON KYLE ROARK. Nucleic acid-driven quantum dot-based lattice formations for biomedical applications.
(Under the direction of DR. KIRILL AFONIN)

We present a versatile biosensing strategy that uses nucleic acids programmed to undergo an isothermal toehold mediated strand displacement in the presence of analyte. This rearrangement results in a double biotinylated duplex formation that induces the rapid aggregation of streptavidin decorated quantum dots (QDs). As biosensor reporters, QDs are advantageous to organic fluorophores and fluorescent proteins due to their enhanced spectral and fluorescence properties. Moreover, the nanoscale regime aids in an enhanced surface area that increase the number of binding of macromolecules, thus making cross-linking possible. The biosensing transduction response, in the current approach, is dictated by the analysis of the natural single particle phenomenon known as fluorescence intermittency, or blinking is the stochastic switching of fluorescence intensity ON (bright) and OFF (dark) states observed in single QD or other fluorophores. In contrast to binary blinking that is typical for single QDs, aggregated QDs exhibit quasi-continuous emission. This change is used as an output for the novel biosensing techniques develop by us. Analysis of blinking traces that can be measured by laser scanning confocal microscopy revealed improved detection of analytes in the picomolar ranges. Additionally, this unique biosensing approach does not require the analyte to cause any fluorescence intensity or color changes. Lastly, this biosensing method can be coupled with therapeutics, such as RNA interference inducers, that can be conditionally released and thus used as a theranostic probes.

ACKNOWLEDGEMENTS

Primarily, I would like to thank my committee (Dr. Kirill Afonin, Dr. Marcus Jones, Dr. Jerry Troutman, Dr. Hansang Cho, and Dr. Yuri Nesmelov) here at UNC-Charlotte. Their patience and understanding, while helping me progress my knowledge for this project is greatly appreciated. The completion of this project would not have been possible without the help of our collaborators. First, I would like to thank Dr. Marcus Jones and Mr. Jose Castaneda for their knowledge, experimental set-up and time with laser scanning confocal microscopy and fluorescence blinking data workup. Additionally, this work would not have been possible without the tremendous collaboration from Dr. Kirsten Wustholtz and her graduate student, Ms. Jenna Tan, at the College of William and Mary. Their hard work and dedication to this project helped us respond to reviewers from ACS Sensors, while our publication was under review. Also, I would like to thank Ms. Morgan Chandler, Mr. Strahinja Talic, and Mr. Ram Jawahar for their hard work and collaboration in either the experiments or the manuscript writing process. Furthermore, Dr. Joseph Tracy and his graduate student, Mr. Brian Lynch, for performing TEM and data analysis on our different DNA-QD lattice assemblies at North Carolina State University. Moreover, Dr. Mathias Viard and the National Cancer Institute for performing some cell culture studies presented in this work. Figures appearing in this work, that were not presented in our publication in ACS Sensors were produced by myself and Ms. Courtney Bishop. Last, but, certainly not least, I would like to thank Dr. Kirill Afonin for the opportunity to work in his lab. Learning all about RNA synthesis, having the individual attention from a principle investigator at universities like UNC-

Charlotte, and the constant meetings have helped me to become a better scientist and professional.

DEDICATION

I would like to dedicate this thesis to my supportive family including: my mother (Christina Kenter), my step father (Rick Kenter), my brother (Kris Roark), and my father (David Roark). I could not have completed this project without the amazing support from my girlfriend, Courtney Bishop, and her family, who worked day and night reading many versions of this thesis and helping with figure design. Lastly, I would like to dedicate this work to Dr. Afonin's lab at UNC-Charlotte for their assistance in this project. Without every single member's support and constructive criticism this thesis would not have been successful.

TABLE OF CONTENTS

LIST OF TABLES

LIST OF FIGURES

LIST OF ABBREVIATIONS

Ago	Argonaute
DNA	deoxyribonucleic acid
DS RNAs	Dicer substrate RNAs
(dsDNA(s))	double-stranded DNAs
eGFP	enhanced green fluorescent protein
gMFI	geometric mean fluorescence intensity
(EtBr)	ethidium bromide
(Glc)	glucose
(GOx)	glucose oxidase
(IDT Inc.,)	Integrated DNA Technologies
(K-*ras*)	Kirsten Rat Sarcoma
LOD	limit of detection
(nt(s))	nucleotide(s)
(PAGE)	polyacrylamide gel electrophoresis
(QD(s))	quantum dot(s)
(RNA)	ribonucleic acid
(RNAi)	RNA interference
(RT)	room temperature
(siRNAs)	short interfering RNAs
(ssDNA(s))	single-stranded DNAs
(SG)	SYBR Green II
(WC)	Watson-Crick

CHAPTER 1: INTRODUCTION

1.1.1 Diagnostics and Biosensing

The diagnosis and early detection of terminal diseases such as cancer, can, in many ways, change the outcome of a patient's prognosis and their rate of survival.[1-3] Many of these diseases can be attributed to the presence of a cellular or physiological abnormality that causes disease progression. For example, high levels of the prostate antigen biomarker has been reported in prostate cancer.[4, 5] The capability to detect trace amounts of biological molecules *in vitro* or *in vivo* with high sensitivity and selectivity with rapid real-time data acquisition can be proficient with biosensors.[6, 7] Biosensors are self-contained analytical devices that use a biological functional component such as, for example, nucleic acids, enzymes, antibodies, cellular receptors, and small molecules that can respond in the presence of a specific analyte. For example, nucleic acids from bacteria or viruses, antigens or antibodies in blood samples, pathogens in food, and pollutants in water, soil, and air can be detected.[7, 8] The sample detection is coupled with a physiochemical transducer.[1, 6, 7, 9] This physicochemical transducer is used to convert the target recognition response into a detectable electrical sign.[6, 7, 10, 11]

The expansion of biosensing research can be partially attributed to the success of glucose sensors[12] for the detection and management of diabetes mellitus[13] and in home pregnancy tests.[1, 14] The first glucose sensor was developed by Clark and Lyon, this oxygen electrode used glucose oxidase (GOx) to oxidize D-glucose (Glc) to D-glucono-lactone and hydrogen peroxide.[7] Many advances have been made to this biosensing strategy, where Hicks and Updike used another electrode without GOx as a reference. Clemens *et a*l. introduced the Biostator for continuous Glc monitoring and by

incorporating charge transfer from tetrathiafluvalene-tetracyanoquinodimethane to cause an electron transfer to GOx to the immobilized electrode.[15-17]

Biosensors are divided into different classifications based on the biological signaling mechanism or the transduction response that is used for detection (Figure 1). Examples include: enzymatic, immunological, cellular, biomimetic, and nucleic acid-based sensors.[6, 11, 18, 19] Similarly, biosensors can be differentiated by the signal transduction response that is implemented. These include: electrochemical, optical-based, piezoelectric, and calorimetric.[6]

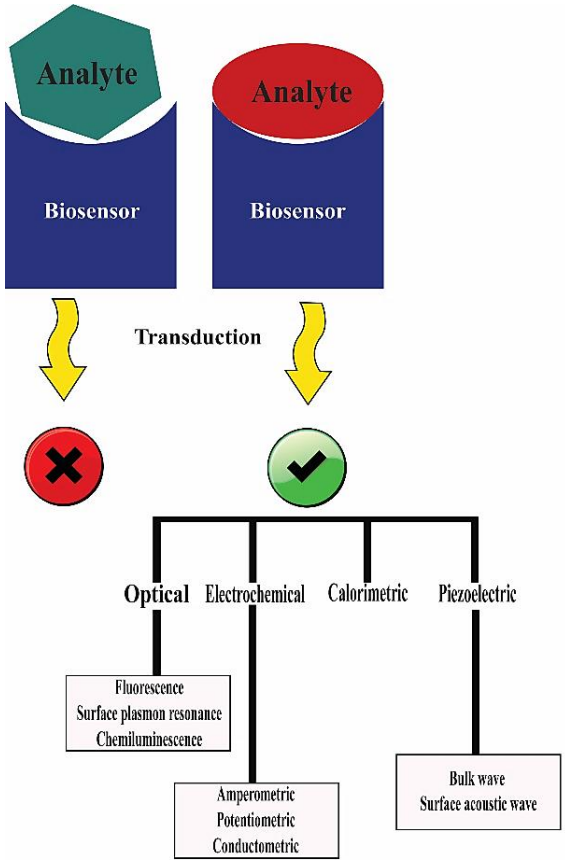

Figure 1: Elements of biosensors. A. By incorporating a biological recognition element (*e.g.*, nucleic acids, whole cells, antibodies, or enzymes) that are either bound or immobilized onto an electrical surface the detection of a target of interest can be selected. *Figure Credit: Kyle Roark and Courtney Bishop*

Optical-based biosensors are one of the common classes of biosensors that are highly investigated, which allow label-free and real time processing.[6, 20] These devices have been implemented into several applications, such as life sciences, food safety, security, and medicine.[21, 22] Optical biosensors can have several different modes of transduction (absorption, fluorescence, Raman, and surface enhanced Raman spectroscopy) with surface plasmon resonance and fluorescence being the most common.[1, 6] Fluorescence is a type of luminescence, which is a product of the energy change from excited to ground state electronic transitions.[6] Different types of luminescence differ by the sources that supply the energy (electromagnetic radiation). Fluorescence involves the excitation of an electron through the absorption of a photon that places an electron from the ground state into a higher excited singlet state ($S_0 \rightarrow S_2$).[23, 24] The molecules undergo a rapid loss of vibrational/rotational energy through collisions with the solvent environment, also known as internal conversion into the higher vibrational levels of the excited singlet state S_1.[23] This can be followed by the emission of a photon with longer wavelength emission known as Stokes' shift, through fluorescence into a vibrational level of the ground state (Figure 2).[23, 24]

However, fluorescence is not always an ideal read out for biosensing due to intersystem crossing into a long-lived triplet state, which can cause non-radiative recombination due to a forbidden transition[23-25] resulting in fluorescence intermittency or blinking. This phenomenon will be further discussed in Chapter 1.2 in relation to quantum dot fluorescence blinking, which has led to a the development of robust biosensing strategy operating through the programmable formation of quantum dot assemblies (lattices).[26]

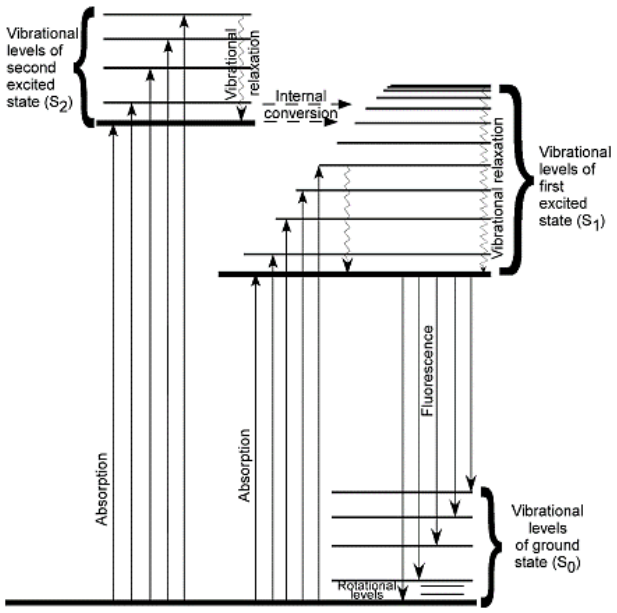

Figure 2: Perrin-Jablonski diagram conveying the mechanism of fluorescence. Where an absorption of a photon into an excited singlet state, is followed by internal conversion into a lower level exited state. Finally, emission of a photon to different vibrational energy levels of the ground state. *This image was adapted from.*[23]

Several new classes of biosensors have been developed, such as metabolism and affinity biosensors.[7] Metabolism sensors refer to the recognition of a target molecule and the chemical reaction conversion to a product that signals the transduction response.[7] In contrast, an affinity sensor encompasses immuno-sensors and aptamers that use hybridization of a bio receptor-analyte interaction complex, which signals the transduction response. For example, an acetylcholinesterase affinity sensor has been used in the recognition of nerve agents that block the enzyme from hydrolyzing acetylcholine and its derivatives when immobilized onto an electric surface.[27]

1.1.2 Nucleic Acid-based Biosensors

To appreciate the experiments presented in Chapter 3, recent advances in nucleic acid biosensor technology will be reviewed in this section. First, there must be a description of the structure of deoxyribonucleic acid (DNA). DNA is composed of four

nucleotides that contain hetero-nitrogenous aromatic rings (adenine, guanine, cytosine, and thymine). These nucleotides can form hydrogen bonds with each other based on the specific complementarity rules (A-T, G=C, known as Watson-Crick (WC) base pairs (Figure 3).[28] These interactions along with Van der Waals contacts of pi-electron clouds of adjacent bases can keep two or more DNA strands together.[29] Continuing, the individual nucleic acids, also referred to as oligos, are cheap, biocompatible, and easily fine-tuned to program the self-assembly of a diverse array of DNA/RNA nanostructures.[30-32] For example, new nucleic acid targets can be detected just by changing the primary sequences and testing the assembly *in silico* through computational suites, such as NUPACK.[33]

Nucleic acid biosensors are advantageous due to the low cost, simple programmability rules, and high assembly efficiency.[21, 34] The rudimentary premise of most nucleic acid biosensors are based on a specific sequence hybridization of immobilized nucleic acid probes with targets, which is achieved by WC base pairing. Three main nucleic acid-based biosensors are found in the literature: DNA sensors, aptamers, and NAzymes.[21] DNA sensors are designed to use the sequence specific mechanism discussed above. Moreover, these reactions are often reversible by changing the ionic strength and temperature.[6]

Aptamers are specifically selected sequences of either DNAs or RNAs that have a high binding affinity for a specified target.[21, 35, 36] Aptamers are selected by using the *in vitro* selection technique, Systematic Evolution of Ligands by EXponential enrichment or SELEX. Briefly, SELEX is used to selectively amplify a DNA or RNA sequences that can specifically bind to the analyte. The SELEX is initiated by using a pool of random

oligonucleotides.[37] These randomized sequences are run through an affinity column with an immobilized target, either proteins or organic molecules.[38, 39] These selected sequences are then amplified by the polymerase chain reaction (PCR) to increase the binding affinity. Aptamers for proteins or the intercalation of ssDNAs have been immobilized on a bio-receptor through thiol or biotin linkages.[13, 21, 40] The utilization of SELEX has aided in design and experimentation of aptamer-based sensors (aptasensors) for the detection of a variety of targets.[7] One of which used a DNA aptamer that were electrostatically bound to poly-L-lysine (PLL) coated AuNPs that produced local surface plasmon resonance and surface-enhanced fluorescence between Cy3B labeled aptamers, unless vascular endothelial growth factor (VEGF) was present.[41] (Figure 3)

Lastly, NAzymes are catalytic nucleic acids that are composed, for example, of a substrate DNAs and an RNA linkage that are branched to an enzymatic strand.[21] When a cofactor is presented, the enzymatic reaction takes place that cleaves the substrate DNAs into two halves.[21] This biosensing approach has been used for the design of sensors using G-rich sequences to form a G-quadruplex that uses peroxidase activity to cleave the products.[21, 42] Chen *et al*, developed a label-free fluorescence biosensor to sense terbium (Tb^{3+}) by using a G-quadruplex. This sensor could detect $Tb^{3+}$with a limit of detection (LOD) of 0.55 pM.[43] (Figure 3)

Recently, nucleic acid sensors have been designed to target the foodborne pathogen, Vibrio cholera,[44] P53 tumor suppressor gene,[45] and breast cancer over expressed c-erbB-2 oncogene.[46] Vibrio cholera has been detected at a limit of 5 ng using targeted biotinylated PCR amplicons that are bound to fluorescein.[44] Continuing, a P53 tumor suppressor gene has been detected using a nicking endonuclease assisted target

recycling and hyper branched rolling circle amplification. This is completed by a $Ru(phen)_3^{2+}$ complex embedded into dsDNA that is released with the assistance of the nicking endonuclease, which transduced an electrochemiluminscence response.[45] Finally, the breast cancer overexpressed oncogene, c-erbB-2, has been sensed by using an exonuclease III-assisted target cycles and long-range assembly DNA concatamers using an up conversion luminescent biosensor.[46]

Many of these biosensing approaches differ by their transduction response.[21] To explain the concept, we will briefly review relevant electrochemical and fluorescence nucleic acid-based biosensing strategies. Electrochemical detection is completed through the immobilization of a ssDNA or hairpin nucleic acid probes onto an electrode that is dispersed in solution.[47] Interactions with the analyte cause the formation of dsDNAs.[47] These hybridization methods can produce a transduction response with a change in current, voltage, or conductivity.[21, 47] In addition, enzymes or redox sensitive labels can cause the transduction. For example, Xuan *et al* measured the difference in diffusivity between a free ferrocene-labeled peptide nucleic acid (Fc-PNA) and a labeled Fc-PNA, which could hybridize to its complementary sequence.[48] This hybridization caused the opening of a stem-loop template for annealing and extension by using DNA polymerase. While Du *et al.* designed a novel E-sensor for reporting human T-lymphotropic Virus Type I gene, which showed an LOD of 25.1 pM.[49] (Figure 3) The next section will discuss quantum dot-based biosensing techniques.

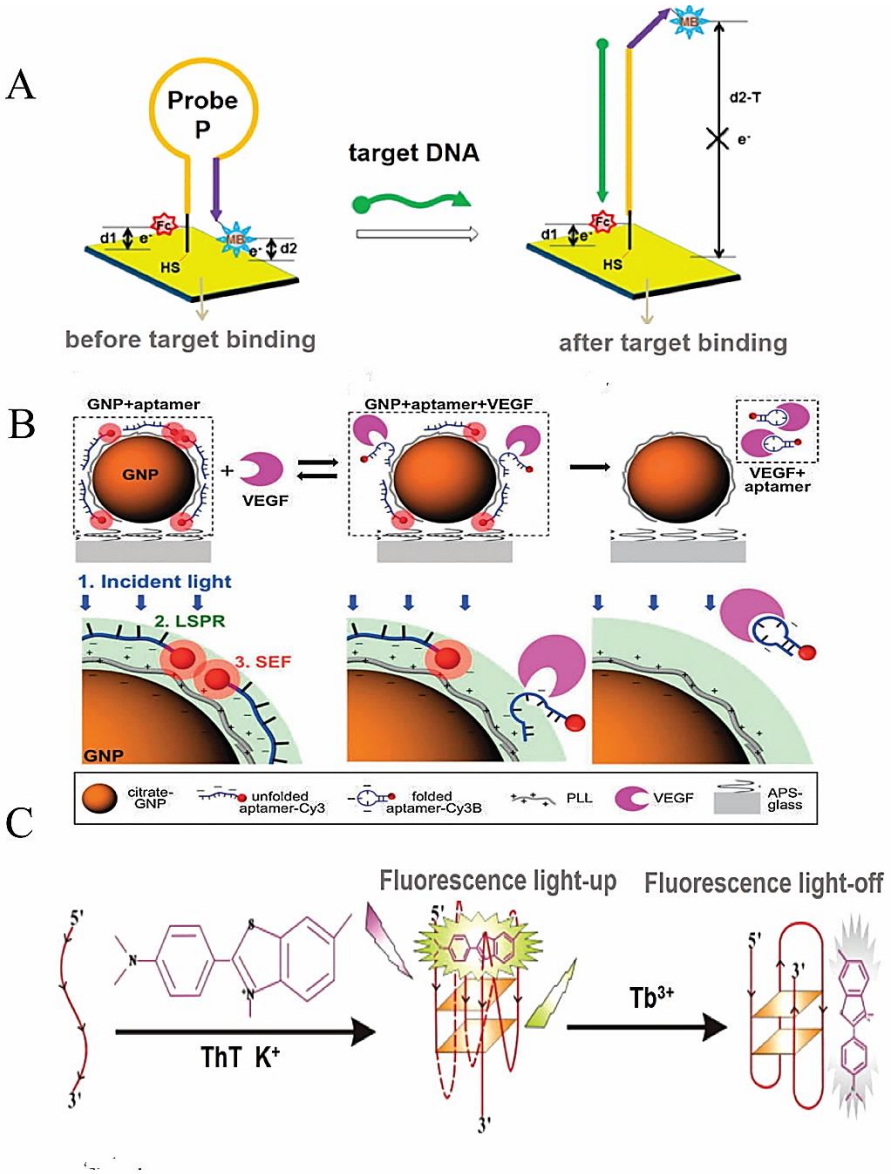

Figure 3: Different types of nucleic acid biosensors. A. By incorporating a nucleic acid hairpin probe, a sequence that is complementary for the loop region, can induce the conformational change of to form a dsDNA that can separate methylene blue and a ferrocene-labeled peptide nucleic acid and transduce an electrical response. *This image was adapted from*[49] B. DNA aptamer labeled with Cy3B for VEGF165 is unfolded when VEGF165 is not present and electrostatically bound to a positively charged PPL-coated gold nanoparticle. When VEGF165 is added, the aptamer binds to the protein and decreases electrostatic local plasmon resonance and surface enhanced fluorescence. *This image was adapted from*[41] C. G-quadruplexes can be used as sensor for the detection of metals such as, terbium which reduced the fluorescence signal through the formation of a G-quadruplex. *This image was adapted from*[43]

1.1.3 Quantum Dot-based Biosensors

Quantum dots (QDs) are colloidal luminescent semiconductor nanocrystals with sizes ranging from 2-10 nm in diameter that have become an invaluable innovation over fluorescent proteins and organic dyes.[50-59] These nanoparticles are composed of a semiconducting core and a shell that protects the QD against oxidation.[60] The size of the nanocrystals become comparable to the Bohr radius, which is the distance between charge carriers (electrons and orbital holes) and is a characteristic of the bulk semi-conducting material.[50, 54, 61] This decrease in space leads to size-tunable optical properties[53, 62, 63] due to quantum confinement (similar to a particle in box from introductory quantum mechanics), which yields narrow, wavelength-specific emission spectra while maintaining a broad excitation range by a single light source (Figure 4) [53, 64]. These properties increase the capability of using multiplexed assays due to a high quantum yield, long fluorescence life time, and large effective Stokes shift, [53, 54, 62] resulting in emission throughout the visible spectrum by just changing the size of the nanoparticle(Figure 4) [26, 50].

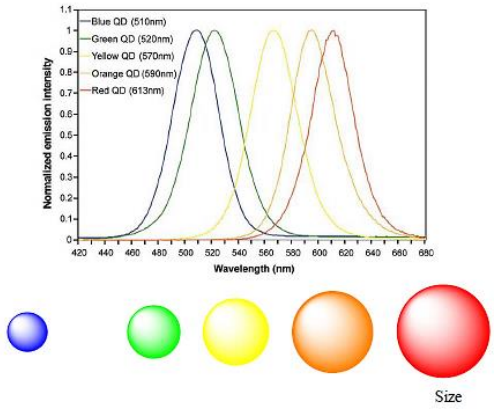

Figure 4: Quantum dot fluorescence and nanoparticle size relationship. Quantum dots are sensitive to size changes due to quantum confinement of charge carriers. The changes in size, changes the band gap energy and affects the energy of the fluorescence emission. *This image was adapted from*[65, 66]

QDs are used in biosensing through the utilization of three main strategies.[53] The first two strategies are designed to use QDs as luminescent labels that can detect target biomolecules through the excitation by photo luminescence(PL), chemiluminescence (CL), or electrochemiluminscence (ECL).[53] The QDs can be bound to certain biomolecules to cause charge or electron transfer processes that either enhances or quenches the QDs fluorescence signal (Figure 5). For example, an ECL sensor was designed to detect the presence alkaline phosphatase through the use an inhibition binding of CdSe nanoparticles (NPs) by phenol.[67] Continuing, glutathione-capped CdSe/ZnS QDs functionalized with methylene blue was used to sense the 1,4-dinitronicotinamide adenine dinucleotide (NADH) through the use of a biotinylated glucose dehydrogenase, which catalyzes Glc to gluconic acid and the quenching of QDs is completed by the oxidized MB^+.[68, 69] Moreover, QD-progesterone antibody conjugate was able to detect progesterone in human serum samples showed comparable results to a commercially available RIA kit.[53, 70]

The final common strategy is the use of resonance energy transfer processes, such as Förster resonance energy transfer (FRET) and bioluminescence luminescence energy transfer (BRET). These resonance energy transfer processes must have an efficient distance between the donor and acceptor and show overlap between the donor absorption spectrum and the acceptor emission spectrum. These sensors are based on either quenching or enhanced illumination when a target is present. Examples include a maltose-binding protein-QD assembly. Medintz *et al*. established a biosensing method to confirm the presence of a protease, the peptide is cleaved in the assembly, thus abolishing FRET and the QD fluorescence is recovered.[71] In addition, Rao and colleagues designed

a nanosensor that used BRET, which utilized the protein, luciferase and the QD as the acceptor.[72] This was completed by using matrix metalloproteinases that caused the cleavage of a linking peptide.[53, 72] The next section will bring aspects of both nucleic acid and QD-based biosensing together to reveal strategies for nucleic acid biosensing using QDs.

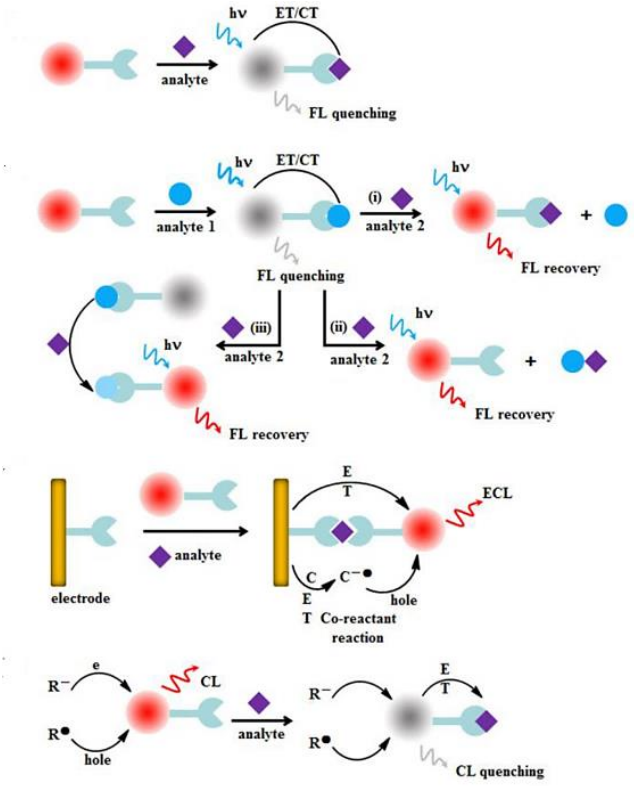

Figure 5: Different types of QD-based biosensors. QD-based biosensors are designed to either go through electron or charge transport in response to a biological molecule. *This image was adapted from*[53]

1.1.4 Nucleic Acid/Quantum Dot-based Biosensors:

In the previous sections, we briefly discussed how nucleic acids and QDs have been incorporated into biosensing strategies. We now combine these strategies together to describe nucleic acid (NA)/QD-based biosensing strategies. Three DNA-QD biosensing approaches have immerged in the literature.[65, 73] The first is based on a "sandwich" system, which uses a target oligonucleotide to bring a QD donor and acceptor into

proximity, that can either quench or induce fluorescence of the QDs. Next, molecular beacons are oligonucleotides that form a stem-and-loop structure.[74] They are based on competitive systems using ssDNA strand displacement to form a more thermodynamically stable dsDNA. A main disadvantage of these biosensing methods, is that they strongly rely on energy transfer processes to change the fluorescence from individual particles, which is not completely ideal due to donor-acceptor distances and changes in the local environment that induce quenching. Finally, as represented in this research and in the literature, competitive assays use a thermodynamically driven strand displacement to form a stable dsDNA, which recovers florescence from the QD by separating it from the quencher.

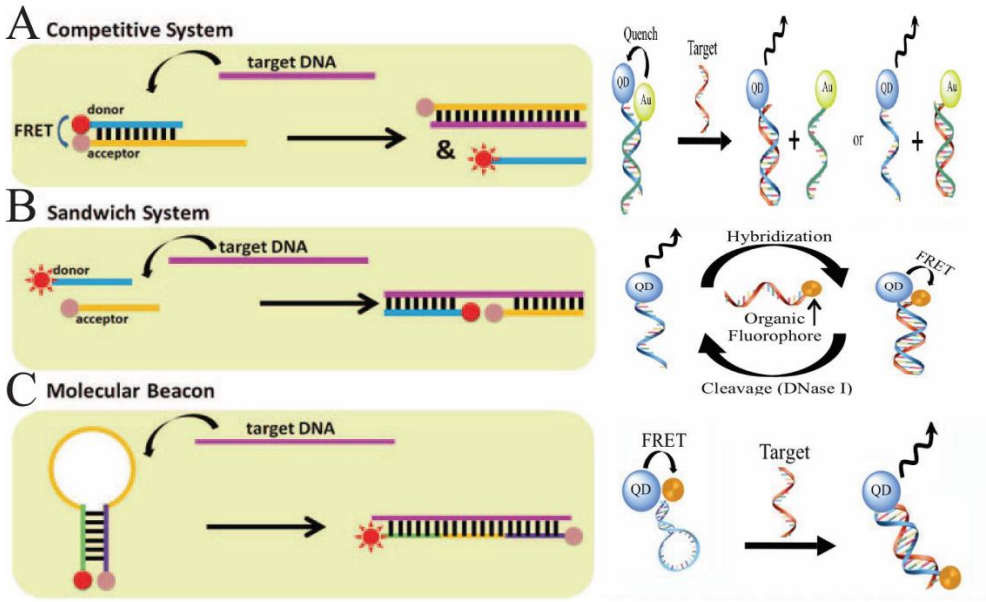

Figure 6: Existing nucleic acid QD-based biosensors. Nucleic acid QD-based biosensing strategies through either competition, sandwich, or molecular beacons. A. Competitive nucleic acid QD-based biosensors uses FRET with a quench for example AuNPs. B. Sandwich hybridization uses a complementary nucleic acid that could either produce FRET to cause the energy transfer and emission of an organic fluorophore. C. FRET is eliminated when a complementary sequence is introduced to a molecular beacon to that is bound to QD, where fluorescence from a QD is restored. *These images were adapted from*[65, 73]

1.2 Fluorescence Intermittency (Blinking) and Biosensing

The formation of an exciton (electron and hole pair) is observed when the excitation energy exceeds the band gap energy (E_g).[65, 75] The weak Coulombic attraction between the electron and holes, can be recombined in either through radiative or non-radiative pathways.[50, 61] For example, a CdSe/ZnS core-shell nanocrystal comprises a linear combination of atomic orbitals on the anion (Se^{2-}), which consists of the highest occupied molecular orbitals (HOMOs) in the valence band, while the cation (Cd^{2+}) is comprised of the lowest unoccupied MOs (LUMOs) in the conduction band. Nanoparticles that are excited by high laser intensities have a higher probability of exciting two pairs of electrons and holes. This involves the charge transfer of an electron from the HOMO to the vacant LUMO, which generates a hole in the HOMO.[61] The repulsion between the electrons and coulombic attraction between one of the electrons and the holes leads to a radiative recombination. The energy that is released through this process is called an Auger process, that is used to ionize the other electron. This is accompanied by electronic and optical properties similar to isolated atoms or molecules, the high efficiency of light emission is largely due to the strong overlap between the electron and hole wavefunctions.[50]

For (QDs), the nano-regime has many attractive advantages that were discussed in Chapter 1.1.3, such as broad absorption, narrow emission, resistance to photo-bleaching, *etc.*[65] However, the nano-sized dimensions are not always advantageous due to surface exposed atoms that can impact the optical properties due to the crystals reduction in size. This reduced size can lead to a crystal facet, which is incompletely bonded and can disrupt the crystalline periodicity that leaves a “dangling orbital”.[50] Furthermore, if these

surface energy states are within the semiconductor band gap, trapping states can result which stabilizes the charge carriers.[58] Moreover, these trap states can manifest in either unsaturated bonds of surface atoms, intrinsic passivating ligands, core-shell interface and even in the surroundings.[58] The trapped charge carriers exhibit reduced mobility and recombination, thus minimizing the overlap of the electron and hole wave functions, which leads to a high probability of non-radiative decay events and impeding charge transport.[50, 58]

This single particle phenomenon is known as fluorescence intermittency or blinking, which is the stochastic switching of fluorescence intensity from an individual molecule between periods of bright, fluorescence cycling (ON states) and periods of dark non-emissive states (OFF states), while under continuous illumination.[58, 76-78] Fluorescent blinking can be observed in single emitters, such as molecular dyes and fluorescent proteins.[58] The literature is in general agreement that the fluorescence blinking arises from charge carrier trapping.[50, 58, 61] However, there is much debate as to how these non-fluorescent periods arise. Two models (Type I and Type II) will be discussed in further detail. Type I model (charging model) assume charge trapping leaves the nanocrystal core effectively charged and can undergo Auger recombination, while the nanocrystal core remains in an ionized state due to a transfer of energy. Type I model is further described by several stages (Figure 7). The first involves the high fluorescence on-state from the cycling of photon absorption and generation of an exciton. The on-to-off follows, which is believed to be caused by thermal- or photoionization, that results in an ionized nanocrystal core due to the excitation of a new exciton. This results in either two holes or two electrons, depending on which charge carrier escaped to the trap state. Then,

off-to-on switching would occur by the return of the trapped charge and neutralization of the nanocrystal.

In contrast, Type II models do not require Auger recombination processes or long-lived trap states and are determined by the trapping site rate, which is very fast compared to a radiative process. This is believed because Auger processes are known to be size dependent, but this is not evident when the lifetimes of the off-state were measured.[58, 79, 80] Instead, in this model, the hole is predicted to be isolated into a trap state that has a life time of ~1 μs, which recombines through a non-radiative process with an electron in the conduction band. This nanocrystal returns to a neutral ground state following each excitation event.

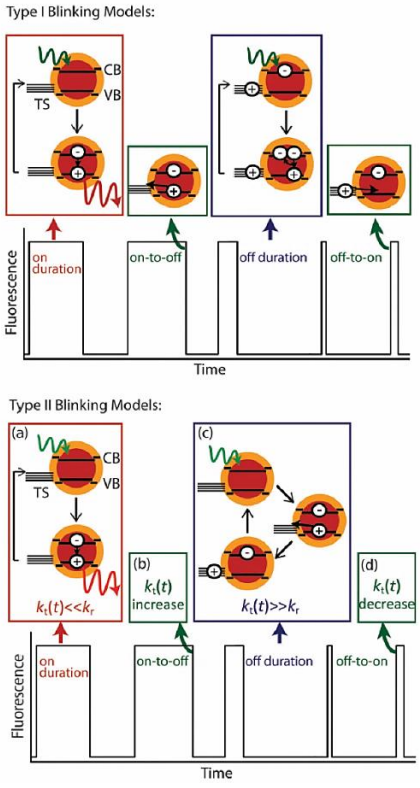

Figure 7: Proposed fluorescence blinking models. *The above image was adapted from*[58]

1.3 Summary:

This section has provided a brief review on the exiting biosensors, which are which are robust analytical devices used for the detection of a variety of biological conditions and molecules. This detection can be coupled to a vast amount of transduction responses, with electrochemical and fluorescence being the most common. Furthermore, by discussing the different types of biosensing methods based on nucleic acids, quantum dots, and the combination of the two, has provided an appreciation of the work presented in the next three chapters.

Our goal in the collaboration between the Dr. Kirill Afonin's and Dr. Marcus Jones' laboratories was to design and test a unique approach to biosensing strategy by using the fluorescence blinking from QDs as output signal. The strategy was designed based of our understanding that blinking, is the single particle phenomenon which becomes obscured when streptavidin-decorated QDs are forced to aggregate through the high binding affinity to double biotinylated DNA duplexes. (Figure 8) This work presents two biosensing assembly strategies denoted as Biosensor Type I and Biosensor Type II. As explained further in Chapter 2, the detection of an oligonucleotide target (a fragment of oncogenic K-*ras*) causes a toehold mediated thermodynamically driven DNA strands displacement. This ssDNA displacement causes the formation of a double biotinylated dsDNA that can induce the aggregation of single streptavidin decorated quantum dots. This work is published in our ACS Sensors.[26] Similarly, Biosensor Type II, which is preparation, utilizes the same nucleic acid target sequence. However, instead of a strand displacement, this assembly forms double-biotinylated DNA trimer assemblies that can turn in crosslink

the QDs functionalized with streptavidin. Lastly, we present preliminary data of the combination of biosensing using fluorescence blinking and the induction of RNA interference using RNA-DNA hybrids that release Dicer Substrate RNAs in the presence of its complementary sequence.

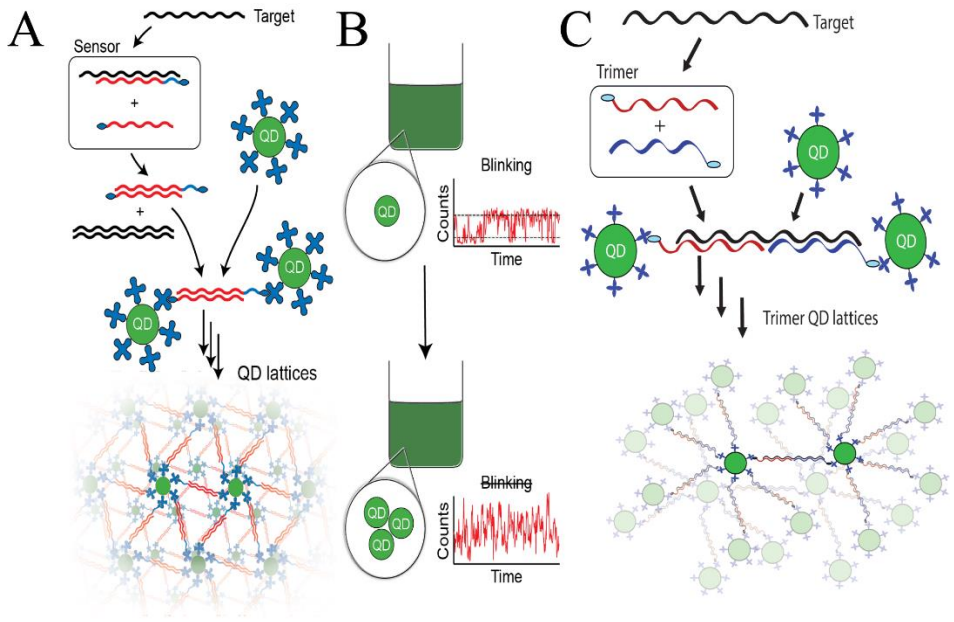

Figure 8: Fluorescence blinking as an output signal for biosensing. A. Biosensing strategies for Type I sensors uses a ssDNA strand displacment to form a double biotinylated DNA duplex. This DNA duplex aggegates single QDs into a QD-DNA lattice. B. Schematic of different blinking traces of single QDs and QD aggregates. *Figure Credit Dr. Marcus Jones* C. Biosensor Type II assembles a DNA trimer that can cross-link QDs to form a QD-DNA lattice. *Figure Credit Courtney Bishop*

CHAPTER 2: EXPERIMENTAL METHODS

2.1 Experimental Overview:

This section describes the design and experimental procedures of assembling and testing two nucleic acid biosensors, designated at Type I and Type II. (Figure 9) These programmable nucleic acids cause the aggregation of single QDs into QD-DNA lattices. Gel electrophoretic techniques were used to confirm the assembly of the nucleic acids and QD-DNA lattices. Additionally, agarose gel electrophoresis, melting curve profile, and transmission electron microscopy was used to test different characteristics of the sensor for example, kinetics, melting temperature, limit of detection, competition assay with molecular biotin, sequence specificity, and DNA distances between three QD lattice assemblies. These studies were completed in conjunction with laser scanning confocal microscopy and fluorescence blinking trajectories to confirm or reject the presence of the target nucleic acid. Lastly, by implementing a designed RNA-DNA hybrid we studied the possibility of using our biosensing method in conjunction with RNA interference for the development of a theranostic probe.

2.2 Materials:

All biotinylated and non-biotinylated single-stranded DNAs (ssDNAs) used in this project were purchased from Integrated DNA Technologies Inc. Streptavidin decorated quantum dots with an emission wavelength of 545 nm were purchased from Thermofisher Scientific at a concentration of 2 μM (Qdot® 545 ITK™ Streptavidin Conjugate Kit, Thermofisher Scientific) with their Qdot™ buffer (2% Bovine Serum Albumin BSA with 50 mM borate buffer pH=8.3, with 0.05% sodium azide). All polyacrylamide gels were produced in-house using 40% acrylamide/bis-acrylamide (19:1

or 29:1) purchased from Fisher Scientific and Bio-Rad. Ammonium persulfate (APS) and N, N, N', N' tetramethylethylenediamine were purchased from Sigma Aldrich and agarose was purchased from AquaPor. 89 mM Tris-borate buffers were used with and without 2 mM ethylenediaminetetraacetic acid (EDTA) for denaturing and native polyacrylamide gel electrophoresis.

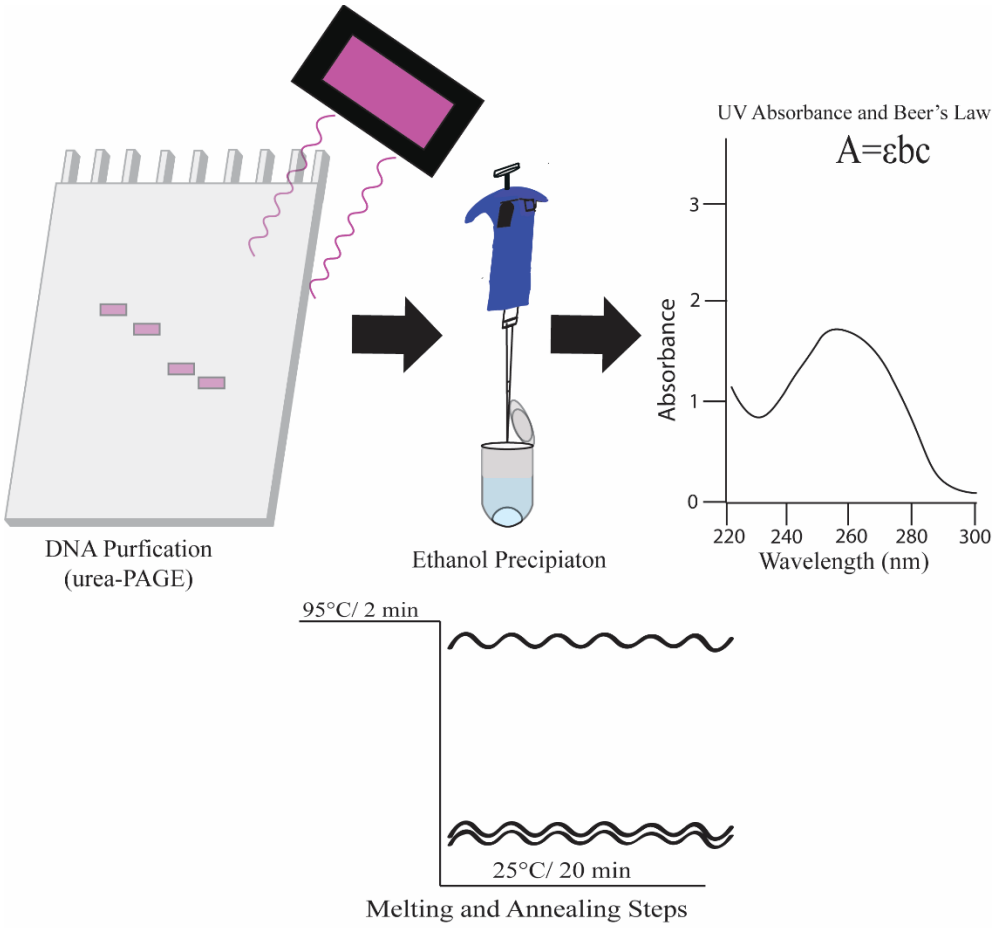

Figure 9: Experimental overview of oligonucleotide biosensor assembly.

Biosensor Type I set up includes four oligonucleotides: 54 nucleotide (nt) mDNA K-*ras* (4) with a mutation of GGT to GAT at codon 12, 51 nt non-biotinylated Guard ssDNA (1), 39 nt biotinylated ssDNA Anti-guard (2), and a 33 nt biotinylated ssDNA DNA for anti-guard (3). Biosensor Type II is presented as preliminary data, and involves

the formation of DNA trimer upon of the addition of a truncated 24 nt (mDNA K-*ras* GGT to GAT at codon 12), 15 nt DNA for antiguard (4), and 15 nt DNA for mRNA K-*ras* (5).

2.3 Rational Design of Biosensor

The sequences and design of the nucleic acid biosensors is presented in this work is schematically described in Figure 5. The design began with the selection of a nucleic acid sequence of interest (K-*ras* mutation in codon 12 GGT →GAT). This was followed by selecting the complementary sequence of each composition step (ordering the reverse complement from IDT). However, to ensure that this assembly is accurate and does not contain secondary structures that would impede the assembly, it is tested using NUPACK.[33]

Sequences (5'→ 3') of oligonucleotides used in this project

Biosensor Type I

Target mDNA K-*ras* (4)

GTAGTTGGAGCTGATGGCGTAGGCAAGAGTGCCTTGACGATACAGCTAATTCAG

Guard ssDNA (1)

CTGAATTAGCTGTATCGTCAAGGCACTCTTGCCTACGCCATCAGCTCCAAC

Anti-guard biotinylated (ssDNA) (2)

BiotinDT-GTTGGAGCTGATGGCGTAGGCAAGAGTGCCTTGACGATA

DNA for anti-guard biotinylated ssDNA (3)

PC-TATCGTCAAGGCACTCTTGCCTACGCCATCAGC

Biosensor Type II

Truncated Target mDNA K-*ras*

TTGGAGCTGATGGCGTAGGCAAGA

Shorter DNA for Anti-guard KRAS (4)

BIOTIN-CACTCTTGCCTACGC

DNA for mRNA KRAS (5)

CATCAGCTCCAACTA-BIOTIN

Dummy Target mDNAs tested as negative control

D1

GGGAGATTTAGTCATTAAGTTTTACAATCCGCTTTGTAATCGTAGTTTGTGT

D2

GGGATCTTTACCTACCACGTTTTGCTGTCTCGTTTGCAGAAGGTCTTTCCGA

RNA/DNA hybrids used for activation of RNAi upon QD lattice formation

DNA strands designed to form RNA/DNA hybrids with sense and antisense strands of Dicer Substrate (DS RNAs) selected against Green Fluorescent Protein or GFP. Once formed, those hybrids will have single stranded toeholds that are designed to interact with each other and to initiate the branch migration. The branch migration will liberate the DS RNAs

Sense (forms Hybrid 1)

pACCCUGAAGUUCAUCUGCACCACCG

Antisense (forms Hybrid 2)

CGGUGGUGCAGAUGAACUUCAGGGUCA

Note: Anti-guard and DNA for anti-guard are complementary. The orientation of 5’ and 3’ are used for ordering from IDT.

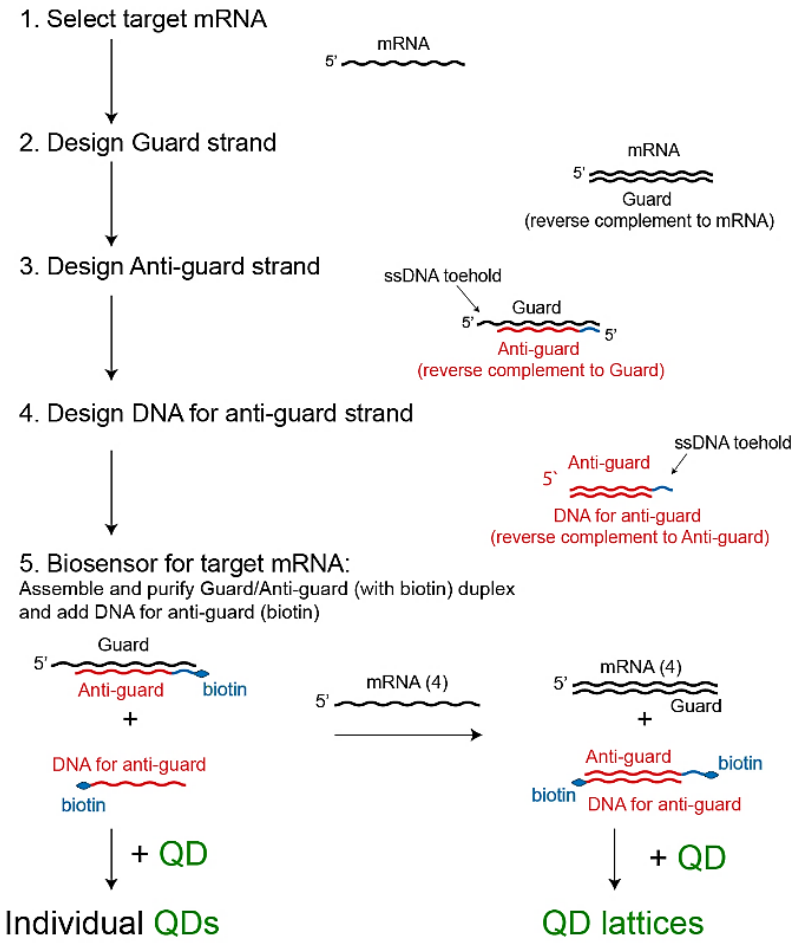

Figure 10: Design schematic of nucleic acid-based biosensor that undergoes single-stranded DNA strand displacement to form a double biotinylated double-stranded DNA. A target sequence is selected, following reverse complements with different thermodynamic stabilities that drive the reaction forward.

2.4 Gel Purification of Purchased Oligos

All oligos were purified using an 8% denaturing polyacrylamide gel electrophoresis (urea-PAGE). This was performed by mixing double-deionized dd_iH_2O 10X TBE, 20% acrylamide/bis-acrylamide/8 M urea, and 8 M urea for a final volume of either 50 or 30 mL. After swirling the beaker, TEMED and 10% APS were added to initiate the free-radical polymerization and carefully poured into the assembled glass plates. Once the gel was polymerized, the DNA strands dissolved in $ddiH_2O$ were mixed in 1:1 ratio of urea loading buffer (8 M urea, 1% bromophenol blue, 1% xylene cyanol,

and 10X TBE). The gel was placed onto the gel rig in 1X TBE and the gel was run between 50-100 Watts. After completion the gel was visualized using a low wavelength ultra violet (UV) lamp (Figure 9A). The gel parts containing the DNAs were excised, transferred into an elution buffer (300 mM NaCl, 10 mM Tris pH=7.5, and 0.5 mM EDTA) and placed to the orbital shaker at 4 °C overnight.

The next day, the eluted DNAs were precipitated by transferring to a solution of 100% ethanol and placed into a -20 °C freezer for 1-3 hrs. The samples were centrifuged for 30 min at 16000g followed by two washing steps with 90% ethanol and centrifugation for 10 min each. Speed vacuum at ~55 °C for 10-15 min was used to evaporate the leftover ethanol, after a pipette was used to remove the excess (Figure 9) and the pellet was dried by using a speed vacuum. The pellet was re-suspended in dd_iH_2O and the absorbance was measured at 260 nm (Figure 9C) using a UV-Vis spectrophotometer (Nanodrop 2000). The concentrations were found by using the Beer-Lambert Law (Figure 9) where IDT's Oligo Analyzer tool determined the extinction coefficients listed for each sequence (Table 1).

Table 1: List of extinction coefficients of the nucleic acid sequences used in this work.

Oligo Sequence	Extinction Coefficient (L/(mol·cm))
Target mDNA K-ras	535100
Guard ssDNA	470400
Anti-guard biotinylated ssDNA	386100
DNA for anti-guard biotinylated ssDNA	301300
D1	506200
D2	475800
Sense_GFP	234200
Antisense_GFP	271000
D_4 Anti-guard KRAS	126800
D_4 mRNA KRAS	142200
Truncated mDNA K-ras	241000

2.5 Biosensor Assembly

2.5.1 Biosensor Type I Assembly

DNA duplex comprised of Guard (1) and Anti-guard ssDNAs (2) were assembled by diluting the oligos into compatible final concentrations (*e.g.*, 10-20 μM) in 1X assembly buffer (50 mM KCl, 2 mM $MgCl_2$ 89 mM tris-borate pH=8.3) to a final volume of 20-30 μL. The DNAs were incubated at 95 °C for two min, then rapidly removed from the heating block to room temperature (RT/25 °C) and incubated for 20 min in the dark at RT. The assembled DNA duplex (1+2) was mixed in equal ratios with DNA for Anti-guard ssDNA (3) and incubated for 20 minutes at 37 °C in the presence of target mDNA K-*ras* (4) to allow the ssDNA strand displacement and the formation of two dsDNAs (1+4) and (2+3).

2.5.2 Biosensor Type II Assembly

DNA trimer comprised of DNA for Anti-guard KRAS (4) and DNA for mRNA KRAS (5), and a fragment of mDNA K-*ras* were assembled by diluting the oligos into compatible final concentrations of 10-20 μM in 1X assembly buffer to a final volume of 20-30 μL. The DNAs were incubated at 95 °C for two min, then removed and cooled to RT. At which time the trimer was equilibrated in the dark for 20 min.

2.6 Electrophoretic Mobility Shift Assays (Agarose Gel Electrophoresis and Native-Polyacrylamide Gel Electrophoresis)

All nucleic acid assemblies and re-association experiments were evaluated at 4 °C on an 8% (19:1) native polyacrylamide gels in the presence of 1X TB with 2 mM $MgCl_2$. Gels were run for 1.5-2 hrs. at 300V, 150 mA, and stained with aqueous ethidium bromide (EtBr) (0.05 mg/mL). The formation of the QD-DNA lattices was analyzed at RT with 2% agarose gels with EtBr. Bio-Rad™ ChemiDoc MP Imaging System (Bio-

Rad, Hercules, CA, USA) was used to visualize QDs (set for 525 nm) and EtBr (set for 605 nm) stained nucleic acids.

2.7 Melting Temperatures of Designed Assemblies

DNA biosensor dsDNAs (1+2), (2+3), and (1+4) were assembled at 2 μM concentrations as described in Chapter 2.4.1 to determine the thermodynamic stability relationship between the nucleic acids. These samples were mixed with 10 μL of 10X SYBR® Green II RNA gel stain (Thermofisher). The mixture was incubated in the dark for 20 min to ensure intercalation. All three dsDNAs were placed into a CFX96 Real-Time™ System coupled with a C1000 Touch™ Thermal Cycler (Bio-Rad™). A melting curve procedure was selected which ranged from 50.0°C-95.0°C, where the plate was read every 0.2 °C for the SYBR Green signal. The data was worked up using OriginPro 2016™ data analysis software where -d(RFU)/dT was plotted as a function of temperature. The melting temperature (T_m) was determined by the peak finding function in OriginPro 2016™ from each negative first derivative plot.

2.8 Nucleic Acid/Quantum Dot-based Biosensor Studies

2.8.1 Titration of Quantum Dots (QDs) with ssDNA

Biotinylated Anti-guard ssDNA of indicated concentrations were prepared through a series of dilutions with Qdot® incubation buffer to determine the saturation point of the biotin-streptavidin interactions between nucleic acids and QDs. These samples were prepared by mixing 20 μL of 0.2 μM QDs in Qdot® incubation buffer were arranged. To get different QD: DNA ratios (1:30, 1:20, 1:15, 1:12, 1:10, 1:8, 1:6, 1:4, 1:2), 2 μL of QDs were mixed with 2 μL of DNAs at: 6.0 μM, 4.0 μM, 3.0 μM, 2.4 μM,

2.0 μM, 1.6 μM, 1.2 μM, 0.80 μM, and 0.40 μM. Mixtures were incubated at 37 °C for 20 min, then loaded onto a 2% agarose gel with EtBr. The gel was run for 20 min at 220 V. All gels were visualized with Bio-Rad™ ChemiDoc MP Imaging System).

2.8.2 Titration of Quantum Dots (QDs) with dsDNA Strands

Biotinylated (Anti-guard + DNA for antiguard) dsDNA were prepared through a series of dilutions with Qdot® incubation buffer to determine the accurate ratio needed to assemble a QD-dsDNA lattice. 20 μL of 0.2 μM QDs in Qdot® incubation buffer were arranged. To get the different QD: DNA ratios (1:20, 1:15, 1:12, 1:10, 1:8, 1:6, 1:4, 1:2, 1:1), 2 μL of QDs were mixed with 2 μL of dsDNAs at: 4.0 μM, 3.0 μM, 2.4 μM, 2.0 μM, 1.6 μM, 1.2 μM, 0.80 μM, 0.40 μM, and 0.20 μM. Assembling's were incubated at 37 °C for 20 min, then loaded onto a 2% agarose gel with EtBr. Free QDs and duplexes were loaded as controls. The gel was run and visualized as described above.

2.8.3 Kinetics Experiments

Time course experiment used to determine the time of lattice formation on mixing of QDs with biotinylated duplexes, biotinylated ssDNAs, and RNA-DNA hybrids. 20 μL of 0.2 μM QDs in incubation buffer were prepared and mixed with 20 μL of 2 μM of biotinylated duplex to obtain a total volume of 40 μL at time point zero. The mixture was incubated at 37 °C and 4.0 μL were aliquoted and snap frozen on dry ice at each time point: 30 secs, 1 min, 2 min, 3 min, 5 min, 10 min, 15 min, 30 min, and 60 min. After 60 min, 1 μL of DNase was added and the mix was additionally incubated for 30 min at 37°C. 4.0 μL of the samples were loaded on 2% agarose gel with EtBr in reverse order, along with free QDs and duplexes as controls. The gel was run and visualized as described above.

2.8.4 QD Lattice Assembly for Visualization with Transmission Electron Microscopy

QD-dsDNA, QD-RNA/DNA hybrids, and QD-ssDNAs were prepared for transmission electron microscopy (TEM) by assembling each lattice separately. The dsDNA assembly was completed by mixing DNA with a 12 nt toehold sense and antisense in 1X assembly buffer. RNA-DNA hybrids were prepared by mixing DNA-RNA sense and DNA-RNA antisense separately in 1X assembly buffer. These duplexes were incubated at 95 °C for 2 minutes and then removed to cool at RT for ~20-30 min. Afterwards, they were with QDs at 2 μM to have a final ratio of 1 QD: 10 dsDNAs or 15 RNA/DNA hybrids. After 30 minutes of equilibration at RT, the samples were mixed in 1:1 ratio and incubated at 37 °C for the either 10 minutes for dsDNA and ~30-60 min for RNA-DNA hybrids. Lastly, QD-ssDNAs by incubating sense and antisense ssDNAs with a 12 nt toehold with two different samples of QDs at a ratio of 15:1. These equilibrated for ~30 min. At which time, the samples were mixed in 1:1 ratio and incubated for ~30-60 min at 37 °C.

All lattices were shipped overnight to North Carolina State University in Raleigh, NC and imaged by TEM. Briefly, 1 μM solutions of QD lattices dispersed in dd_iH_2O, 1X assembly buffer, and Qdot buffer were diluted to 0.5 mL each. A glass pipette was used to place one drop of each solution onto a Cu TEM grid with an ultrathin carbon and Formvar coating. After evaporation of the solvent, the samples were imaged with JEOL 2000X transmission electron microscope operated at 200 kV. The distances between the edges of the QD cores were measured using ImageJ software by drawing a line between two QDs.

2.8.5 Limit of Detection Experiments

Series of dilutions of pre-formed QD-dsDNA lattices to determine the lowest concentration of lattices suitable for visual assessment. QD lattices (1:20 ratio of QD: DNA duplex) were prepared as described above. Series of dilutions with Qdot® buffer were performed to get the following concentrations of DNAs: 2.50 μM, 1.25 μM, 0.625 μM, 0.313 μM, 0.0781 μM, 0.0391 μM, 0.0195 μM, 0.00976 μM, 0.00488 μM, and 0.00244 μM. Diluted samples (5 μL) were run and visualized as described above. The free QDs were used as the control.

2.8.6 Competition Assays

Biotin Competing DNA Agarose Gel. Three samples were prepared (100 nM QDs for 1.5 μM ssDNA (3), 100 nM QDs for 1 μM duplex (2+3), and 100 nM QDs for 1 μM duplex (2+3) in the presence of 50 μM of biotin and incubated at 37.0°C for 20 min. Samples were analyzed on agarose gels as described above.

2.8.7 Temperature Dependent Biosensor/Lattice Formation

Analysis of biosensors. After incubation for 20 min of target strand and prepared biosensors (Guard/Anti-guard duplex and DNA for anti-guard) at different temperatures (20°C, 37°C, 45°C, 50°C, and 55°C), samples were incubated with QDs. Based on titration experiments, the optimal QD to Biosensor ratio was chosen to be 1:10 (1:6 and 1:15 ratios were also tested). Samples were incubated for 30 min at 37°C and run on a 2% agarose gel (89 mM Tris, 80 mM boric acid, 2 mM EDTA, and pH 8.3).

2.9 Laser Scanning Confocal Microscopy and Time-Resolved Fluorescence

2.9.1 Spin-coating and Optical Alignment of Confocal Microscope

QD-biosensor solutions before and after incubation with target strands were prepared for confocal imaging by diluting 1-2 μL by two or three orders of magnitude

with Qdot® incubation buffer and were kept on ice until the moment of deposition. Diluted solutions (~20 μL) were spin coated onto methanol cleaned 18 × 18 mm coverslips (Ted Pella, Inc.) with use of a Chemat KW-4A spin coater with the following 2-stage spin settings of 2,500 rpm for 2 seconds (Stage 1) and 3,000 rpm for 30 seconds (Stage 2). The prepared coverslips were mounted onto a Nano-PDQ375 x-y-z translation stage for laser scanning confocal microscopy.

Excitation was provided by a PicoQuant PDL 800-B pulsed laser with an LDH-Series 470 nm laser head at a 10 MHz repetition frequency and power of 1.15 μW. Excitation pulses were coupled into a single-mode optical fiber, then directed to a 500 nm cutoff dichroic beam splitter before being focused onto the sample by a Zeiss 100× 1.25 NA oil immersion objective lens. Fluorescence from the sample was collected through the same objective and directed toward a bandpass filter with a 45 nm width centered about 535 nm before reaching a flip mirror. Orientation of this flip mirror either directed fluorescence toward a Melles Griot 160/0.17 objective lens that focused the signal onto a EG & E Single Photon Counting Module (SPCM) for imaging, or to a Nikon 10× objective lens that focused signal onto a PicoQuant PDM Series Single Photon Avalanche Photodiode (SPAD) for collection of blinking dynamics.

2.9.2 Data Acquisition Using Home-Built Lab View and Fluorescence Blinking Traces

Experimental control and data acquisition was achieved using a homebuilt LabVIEW program. Size and scanning rate for images was 512 ×512 pixels at 5 lines per second. ImageJ was used for image analysis. Detection signals from the SPAD were sent to a Time-Harp200 PCI Card operating in time tagged time-resolved mode, and blinking data were recorded for 180 seconds at each bright spot. Photon macro times were

organized into 10 ms bins to yield blinking trajectories from which intensity histograms were produced.

2.9.3 Cell Culture Experiments

Briefly, RNA-DNA hybrids (sense and antisense) bound to QDs were prepared at UNCC as in Chapter 2.4.3. These hybrids (10X or 50X) were pre-incubated with lipofectamine 2000 (purchased from Invitrogen) at 30 °C into a human breast cancer cell line MDA-MB-231 with/without GFP (grown in D-MEM media (Gibco BRL) that was supplemented with 10% fetal bovine serum (FBS) and penicillin-streptomycin (pen-strep) in a 5% CO_2 incubator). Before each transfection, the cell media was replaced with OPTI-MEM and the prepared 10X or 50X hybrids complexes were added to a final concentration of 1X. The cells were left to incubate for 4 hrs., which was followed by the media change using D-MEM, 10%FBS, and 1% pen-strep.

2.9.4 Flow Cytometry

Transfection and of QD-hybrid sense and QD-hybrid antisense were quantified by fluorescence-activated cell sorting (FACS) by using a FACScalibur flow cytometer (BD Bioscience). Similarly, silencing of MDA-MB-231 expressing eGFP were quantified using FACS. The cells were grown in 12-well plates ($10x10^4$ cells per well) and lifted off using cell dissociation buffer. This was followed by two washing steps by lifting the cells off and washing with PBS. Afterwards, the cells were loaded into the flow cytometer and at least 20,000 events were collected and analyzed.

2.10 Summary:

The experimental procedures outlined above were used for the assembly of nucleic acid biosensors and nucleic acid-QD lattice assemblies. Assembly was confirmed

by utilizing two gel electrophoresis techniques (native-PAGE and agarose gel electrophoresis) using both kinetics and titrations. In addition, several assays (limit of detection, biotin competition, and temperature dependence) were used to evaluate characteristics of the sensor. Lastly, sensor-QD assemblies were visualized using laser scanning confocal microscopy coupled with time-resolved fluorescence to collect fluorescence blinking traces. Future preliminary experiments of uptake and silencing of RNA-DNA hybrid re-association and the formation of QD-DNA lattices and causing the release of DS RNAs was presented to show the possibility of the use of a theranostic probe. Presented next will be the results that follow each of these experimental methods.

CHAPTER 3: RESULTS AND DISCUSSION

This chapter will present nucleic acid biosensor designs shown in Figure 11, characterization using agarose gel electrophoresis, melting temperature of different DNA duplexes, and native-PAGE to visualize the formation of the sensor. Additionally, we present reasonable controls to confirm that our biosensor is assembling the way it is designed to. We further present confocal fluorescence microscopy images of our sensor with and without the presence of the target nucleic acid. The blinking traces reveal how this novel sensor can be used to distinguish between quantum dot lattices that are formed from the formation of double-biotinylated DNA duplexes. We have demonstrated a unique and versatile strategy by using quantum dot fluorescence blinking as an output for biosensing by designing three nucleic acid sensors. One biosensor's design of which was published in our recent papers[26] and the other two are still being investigated.

3.1 Design of Biosensors and Confirmation of Structures

We designed a proof of concept nucleic acid QD-based biosensor that incorporates a total of 4 ssDNAs (Guard (1), Anti-guard (2), DNA for anti-guard (3), and Target mDNA K-*ras* (4) (Figure 5A). These assemblies were testing using NUPACK[33]. The sequence of interest was input into NUPACK.org Analysis tab. The temperature of the complexes was set to be 37.0 °C for each sensor and nucleic acid assembly (Figure 11) with the corresponding minimum free energy of the secondary structure was found.

Briefly, a target (4) can interact with an assembled single-biotinylated DNA duplex (1+2) that was formed by standard melting and annealing procedures completed at room temperature (25 °C). This DNA duplex (1+2) contains a 12 nt ssDNA toehold on the 5' end of Guard DNA. The free energies of the secondary structure of (1+2) was calculated

to be -77 kcal/mol using NUPACK[33] as was described in Chapter 2. Strand (3) is a biotinylated ssDNA that is present in the biosensor, but a difference in -12 kcal/mol prevents the formation of dsDNA (2+3) (-65 kcal/mol) in the biosensor set up ((1+2) +3).

However, in the presence of (4) the formation of (2+3) is more favorable by -85 kcal/mol, which is formed by releasing (2). (2) is singly biotinylated and can interact with its complementary strand (3), which allows the formation of double biotinylated DNA duplex (2+3). Double-stranded DNA duplex (2+3) formation is driven by (1+4) association which is more stable (-97 kcal/mol) due to the gain of 12 base pairs.[26] This double biotinylated DNA duplex can be cross-linked by SA decorated QDs, forming QD lattices due to the chemistry discussed in Chapter 3. This approach does not utilize charge and electronic transfer strategies seen in other quantum dot biosensors found in the literature that was also discussed in Chapter 1.

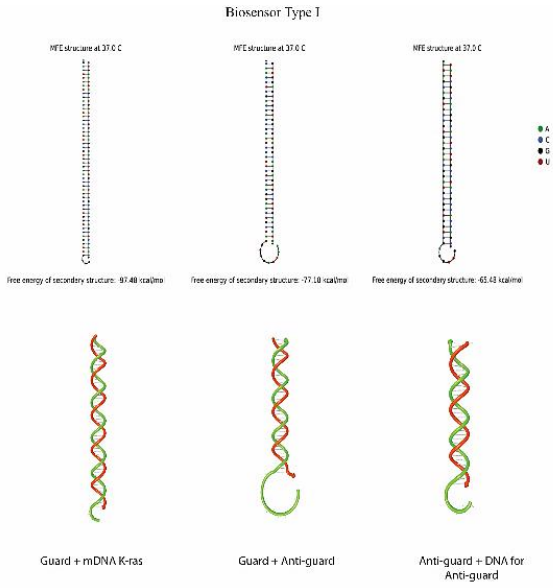

Figure 11: Secondary structures of assemblies predicted with NUPACK.

3.2 Purification of Purchased Oligos:

Purification of purchased oligos was completed by using urea-PAGE (Figure 12). The DNAs were run through a polyacrylamide gel until a separation of 2-5 inches observed between the xylene cyanol (upper light blue band) and bromophenol blue (lower dark blue band). Nucleic acids absorb at 260 nm, and by irradiating the gel on a silica plate allows the quenching of the lamp UV irradiation. The appearance of faint purple bands (between the two dyes) indicates the presence of purified nucleic acids.

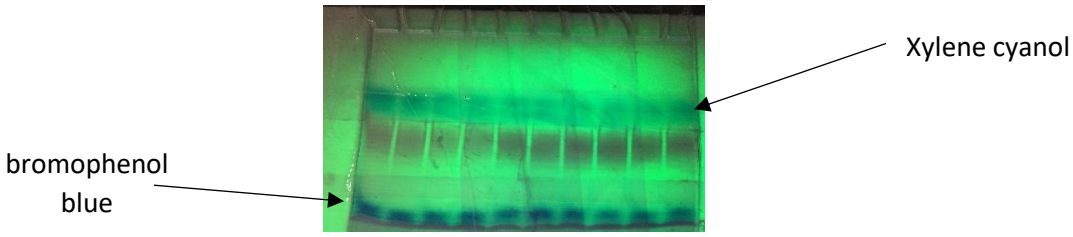

Figure 12: Oligonucleotide purification by urea-PAGE. Polyacrylamide gel showing the separation of ~2-5 inches of control dyes (xylene cyanol and bromophenol blue). The oligonucleotides absorb at 260 nm and appear as faint purple bands that can be excised by a scalpel.

3.3 Analysis of Re-association of Biosensor DNA Strands on Native-PAGE

To assess the association of the DNAs that make up the type I and type II biosensors, native-PAGE was used to analyze several assemblies at different incubation temperatures along with the ssDNA controls (Figure 13). The release of the double biotinylated duplex (2+3) is seen by the formation of two bands when the target (4) is added to the biosensor ((1+2) +3). (Figure 13) These duplexes were released most efficiently at physiological temperature of 37 °C.

In contrast, biosensor type II does not undergo a ssDNA displacement, instead all three oligos that enter the composition of the biosensor form a DNA trimer, seen by the migration of the major band (Figure 13). A truncated sensor was tested which revealed the same efficiency for biosensor type II assembly. However, it was suspected that the

truncated sensor, might aid in the biotin-streptavidin interaction between the QDs and biotinylated ssDNAs. It was hypothesized that the long 12 nt ssDNA region, also known as a toehold of the longer target could have been experiencing steric interactions and not allowing the association between biotin and streptavidin.

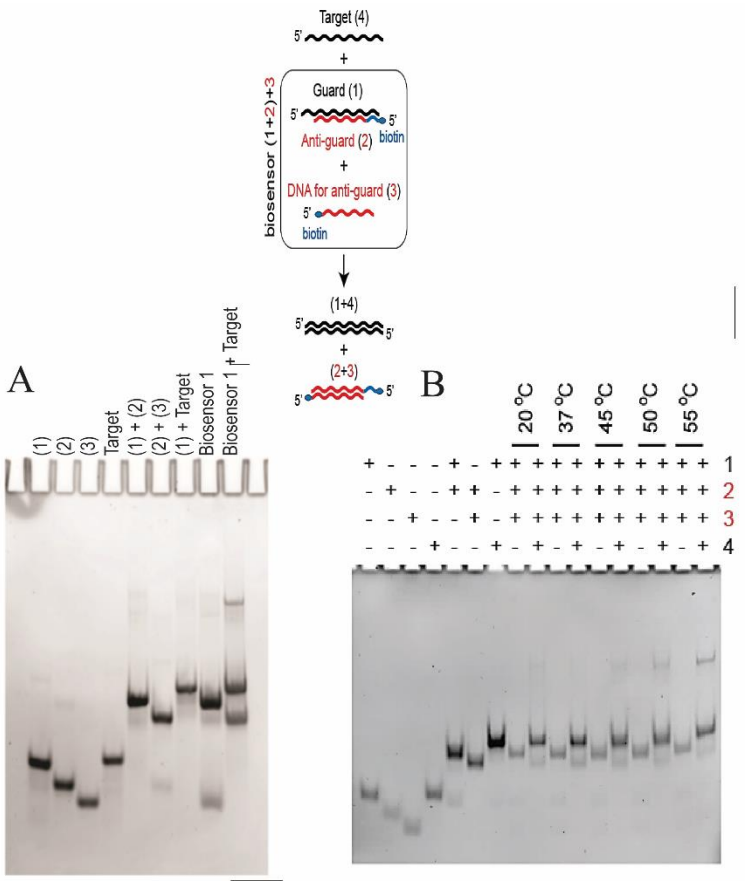

Figure 13: Native-PAGE showing biosensor assembly and assembly of biosensor Type I at varying temperatures. A. Biosensor Type I reveal that when the target is present, causes a toehold-mediated ssDNA displacement to form two biotinylated dsDNAs. B. Biosensor type I was incubated at varying temperatures and it was determined that between 20-37 °C was the most efficient assembly.

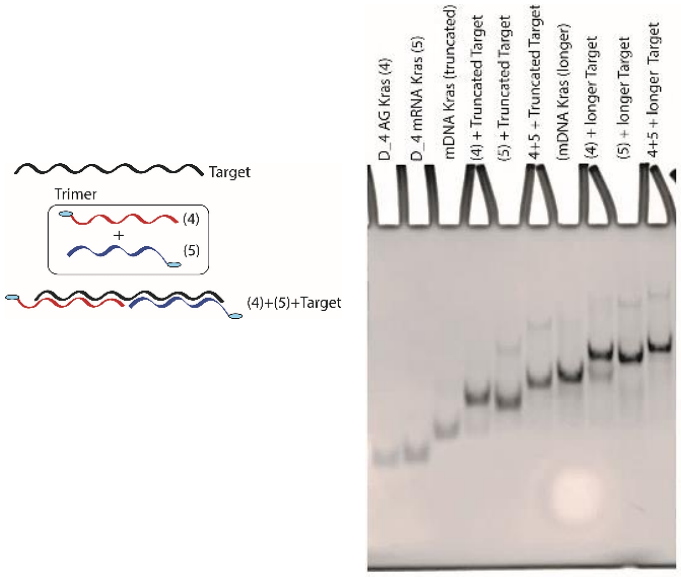

Figure 14: Biosensor Type II and the formation of a DNA trimer observed on native-PAGE. Two different targets were selected (longer target is the same as in Type I), while a 24 nt was believed to eliminate undesired ssDNA interactions that might have been impeding the biotin-streptavidin interaction.

3.4 Melting Temperature Studies

As shown in Chapter 3.1, the thermodynamic stability can be predicted for nucleic acid secondary structures using computational approaches. However, it is essential to confirm these thermodynamic properties through experimentation. The straightest forward procedure for doing this is to determine the melting temperature (T_m) of nucleic acids by measuring the absorbance at 260 nm as a function of the temperature, known as UV-melt. As the temperature is gradually increased, the thermal energy begins to melt the DNA by breaking the intermolecular hydrogen bonds between the nucleotides, exposing the aromatic bases to the UV radiation, which increases the absorbance (hyperchromacity)[81] More precisely, the melting temperature is the temperature at which half of the hydrogen bonds within a certain nucleic acid are melting. These hydrogen bonding (intermolecular forces) are strongly influenced by the primary sequence, size,

charge, and the presence of secondary structure and tertiary interactions.[82, 83] Not only can this temperature provide reasonable predictions for the thermodynamic stability, but by using the vant' Hoff relation, other thermodynamic properties such as enthalpy (ΔH) and entropy (ΔS) can be determined by measuring the melting temperature at varying concentrations of the same sample. Moreover, by plotting a linear relation of 1/T vs. ln (C_t) the slope is used to determine ΔH and the y-intercept is used to determine ΔS, respectively.[84] Other approaches to determine the melting temperature are found in the literature. Such approaches use SYBR Green II fluorescence as a function of temperature using a real-time thermocycler instrument.

This method has become more common due to the limited frequent unresolved melting transitions that occur in complex nucleic acid structures. SYBR Green II has shown an increased sensitivity for nucleic acids, which makes SG useful for fluorescence melting temperature assays.[85] The negative first derivative plot of the DNA duplexes incubated with SYBR Green II (Figure 15) showed values that agreed well with the predicted melting temperatures using IDT's oligo analyzer software. However, the former approach using UV melt was also tried. Unfortunately, results did not match that of predicted melting temperature from IDT's oligo analyzer, as well as the SYBR Green II assay did (Figure 15).

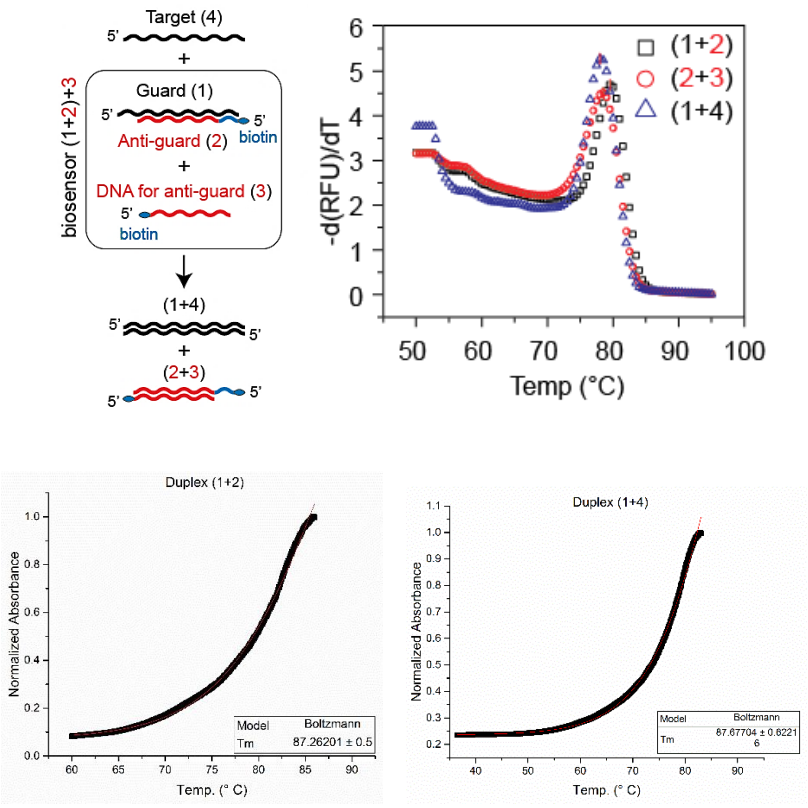

Figure 15: Melting temperature of DNA duplexes in biosensor type I. The negative first derivative plot was used to show the relative thermodynamic stabilities of the DNA duplexes assembled either during or after biosensor I re-association.

3.5 QD Titration Experiments

Several questions arose when investigating biosensor one. One main problem associated with QD lattice formations is over saturation of the streptavidin-biotin interactions. If the streptavidin-decorated QDs are over saturated with biotin molecules, then the formation of the QD lattices can be hindered. The first assay to be completed was a titration of QDs with ssDNAs Anti-guard (2). This experiment was used to determine which ratio the QDs are saturated by the ssDNAs (Figure 15A). The negative charge on the QDs brought about by the binding of the ssDNAs allowed a dramatic increase in the migration rate on the agarose gel. It was revealed that the maximum number of streptavidin-biotin interactions per QD was ~15-20. It was also observed that

the QDs are saturated when ~30 ssDNAs are bound to a QD. The apparent faint red bands seen in the same location as the ssDNA (2) control in the 1:30 ratio (Figure 15A) is a further indication of the saturation point being reach due to an overabundance of ssDNAs and no biotin binding sites remaining on streptavidin. Next, the QD lattice formations were analyzed by titrating QDs with double biotinylated DNA duplex (2+3). We found that the minimum ratio for the formation of the QD lattice was four DNA duplexes: 1 QD and that maximum amount of formation without over saturation was 10 DNA duplex: 1 QD (Figure 15B). Next, it was important to study the kinetics of lattice formation to expedite the assembly of the biosensors, without deteriorating the quality.

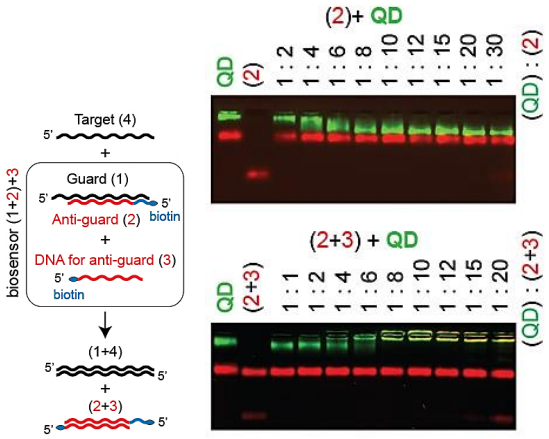

Figure 16: Titration experiments of ssDNAs to determine maximum saturation points and dsDNA to determine maximum ratio of efficiency. A. Titration of Anti-guard ssDNAs with QDs showed that the QDs are saturated with 15 ssDNAs bound to the QDs and completely saturated at a ratio of 1:20, which indicated that the QDs contain ~5-6 streptavidin proteins. B. Titration of double biotinylated dsDNA (2+3) with QDs determined the most efficient ratio to for lattice formation 1:10.

3.6 QD Time-Course

Kinetic assays were performed to determine the time required for the quantum dot lattice assembly when the QDs were incubated with the assembled double-biotinylated DNA duplex, complementary ssDNAs, and RNA-DNA hybrids (Figure 16). It was determined that the preassembled DNA duplexes (either (2+3) or DNA_12) formed the

fastest (within 0.5 min.). In contrast, when QDs were incubated with ssDNAs and RNA-DNA hybrids that had to be re-associated through WC base pairing, the time for full lattice assembly was completed within 30-60 min for complementary ssDNAs and 60-120 min for RNA-DNA hybrids with the full release of DS RNAs. In these assemblies the ssDNAs and RNA-DNA hybrids are bound to two different samples of QDs and allowed to equilibrate before being mixed with their complementary assembly. The major kinetics difference is believed to be due to the time required for the ssDNAs and the DNA toeholds of the RNA-DNA hybrid to find its complementary counterpart and form the assembly in solution. (Figure 16B)

Additionally, each assembly was confirmed to be driven by the DNAs by using commercially available RQ1 DNase (Promega) was added, and caused the release of QDs with shorter DNA fragments. This assay also aided us in optimizing the procedure through shorter incubation times for the preparation of QD lattices for downstream applications exemplified in uptake and silencing experiments. (Chapter 4)

3.7 QD-DNA Lattice Transmission Electron Microscopy

Lastly, transmission electron microscopy images of the three assemblies were completed at NCSU in collaboration with us. Three different buffers were used for the assemblies and dilutions (Qdot buffer, 1X assembly, and dd_iH_2O) this was to determine the stability of the lattices in different buffers and the ease of TEM imaging due to problems arising from viscosity and BSA in Qdot™ buffer. It was concluded that the average distance between 50 QDs for the DNA duplex was 17.7 nm, the distance between RNA/DNA assembled lattices was between 13.7-17.0 nm in, 1X assembly, dd_iH_2O, and Qdot buffer. Finally, the average distance for ssDNA lattice assembly was 15.8 nm.

These values agree well the average distance between QDs is ~15-20 nm due to the 39 nts that have a separation of B-form DNA helix of 0.34 nm ($i.e., 39\ nts\ x\ (0.34\ nm) = 13.26\ nm + \sim 5\ nm\ diameter\ of\ streptavidin = 18.26\ nm$)

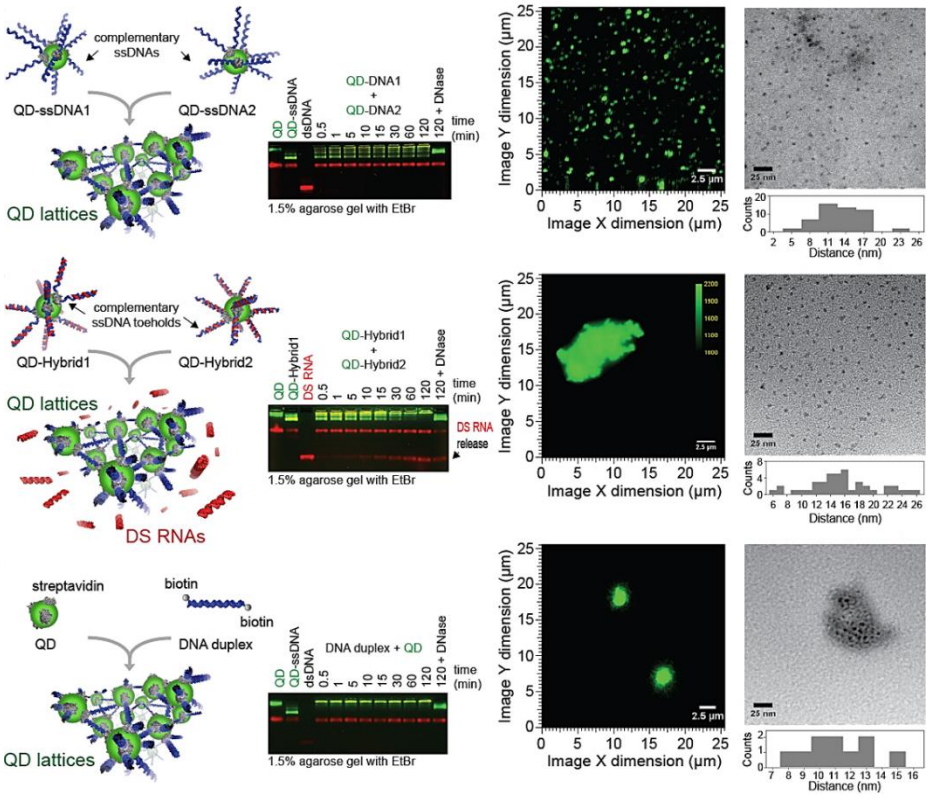

Figure 17: QD-DNA lattice assemblies by three different approaches using ssDNAs, RNA-DNA hybrids, and dsDNAs. A. Agarose gel electrophoresis kinetics assays showed that the different lattice assemblies have different kinetics due to the time of complementary base pairing. B. Confocal fluorescence micrographs show the relative size of lattices due to the QD fluorescence. C. Transmission electron micrographs confirms that the distance between the lattices agrees well with the nucleotide distance between QDs and the average diameter of a streptavidin protein.

3.8 Limit of Detection, Specificity, and Biotin Competition

The limit of detection of target (4) in biosensor Type I was determined by titrating the biosensor with QDs through a series of dilutions with different amounts of (4) which revealed that lowest concentration to detect the formation of the lattice or limit of detection was approximately between 300-350 nM. (Figure 18) This was rather encouraging, however, other QD-based sensors can operate in the pico and femto molar scales, many of these are not optical, but electrochemical sensors.[8, 10, 17, 40] As will be

discussed below, by using laser scanning confocal fluorescence microscopy the limit of detection of target (4) with biosensor type I can be found in this range. Additionally, by using two different "dummy" target strands of similar length, we confirmed that the sensor is specific for mDNA K-ras target (4) by observing no lattice formation with the dummy DNAs (Figure 18). Finally, by adding the small molecule, biotin, we determined that the binding of DNAs to QDs and the formation of lattices was controlled by biotin-streptavidin interactions, by competing with 500 times excess of biotin than the quantum dot final concentration (100 nM), the lattice assembly was completely obstructed. (Figure 18).

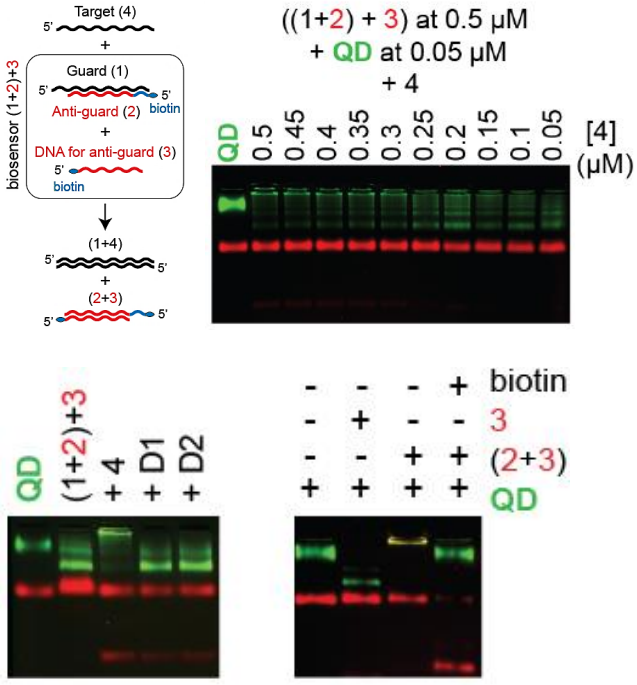

Figure 18: Limit of detection, sequence specificity, and biotin competition.

3.9 Confocal Fluorescence Micrographs and Quantum Dot Fluorescence Blinking

Fluorescence micrographs (Figure 18A-B) using a confocal microscope measured fluorescence intensity signal as a function of time was used to image streptavidin

decorated QDs with biosensor Type I with and without target mDNA K-*ras*. The samples were diluted to ~100 picomolar concentration before being spin-coated onto a quartz coverslip. The images were scaled to the same size (75 µm) and intensity. However, spot size could not distinguish the lattices alone, despite a few brighter spots. Smaller regions from the images in figure 18A-B are shown in Figure 18C-D, which shows streaking of the non-aggregated QDs due to the vertical raster scanning of the x-y- z piezoelectric stage and is strong evidence of non-aggregated QDs. In addition, >90% of the observed particles exhibited single QD blinking dynamics, while a trivial amount localized into small groups, partly due to the hydrophobic character of QDs (data not shown).

Representative fluorescence blinking traces were analyzed on bright spots from Figure A-B. These traces provided significant evidence for the formation of DNA-QD lattices (Figure 20A-D). The blue trace shows random fluctuations between bright (~380 counts/10 ms bin period) and dark (~90 counts/10 ms bin period). In addition, different temperature, and ratios of the DNA-QD lattices are shown in Figure 21. These traces show two intensity histogram distribution where the blue trace shows binary blinking statistics, whereas the red trace intensity fluctuates over a much wider range, indicating the lattice formation. Moreover, we used a binomial model (assuming stochastic and independent blinking from each QD in a lattice) to predict the expected blinking histograms for QD lattices. The histogram shown in Figure 22 calculate the distribution of two-ten QDs in a lattice. QD lattices with six closely resembles the intensity distribution found in Figure 20D.

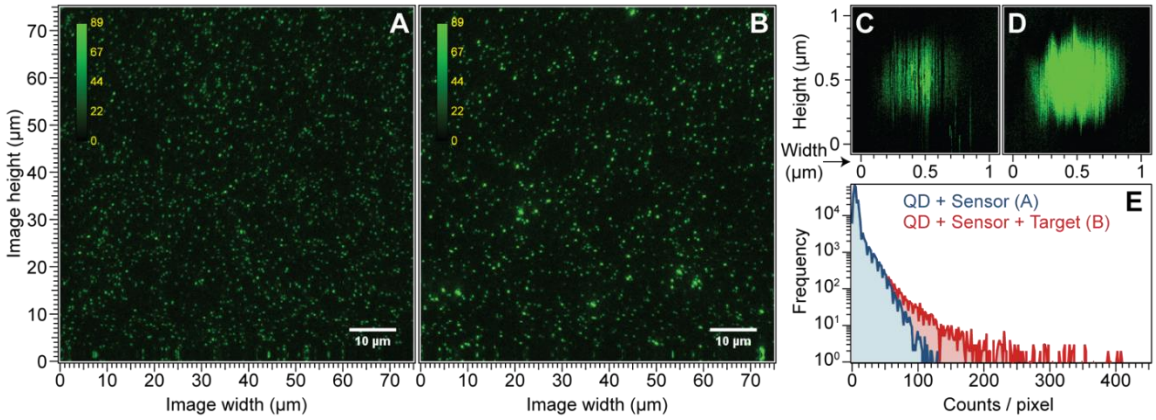

Figure 19**:** Fluorescence micrographs of biosensors with and without target with QDs A: QDs incubated with the biosensor without target added. (1:10 ratio). B: QDs incubated with biosensor after addition of target strand. C: One spot of a Single QD biosensor without target was reimaged from the field in 19A, which exhibits streaking due to blinking phenomenon. D: QD aggregate from 19B, exhibits little to no streaking E: Fluorescence Intensity histograms averaged from 19A and19B. *This image was adapted from our publication.*[26]

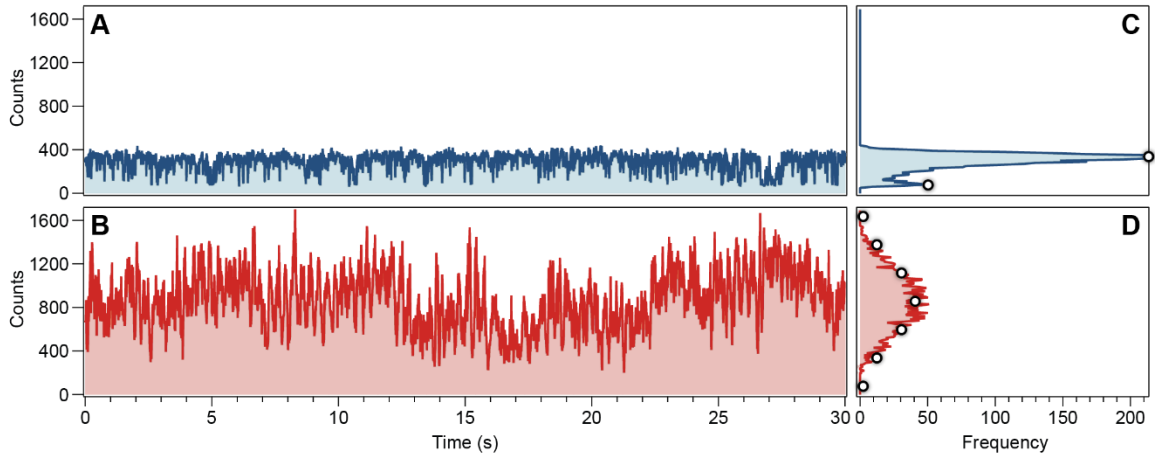

Figure 20: Representative blinking trajectories. A: Blinking trace recorded on a bright spot in a fluorescence micrograph from QDs incubated with biosensor (1:10 ratio). B: Blinking trace recorded on a bright spot from QDs plus biosensor after addition of target strands. Corresponding intensity histograms are shown in C and D. *This image was adapted from our publication.*[26]

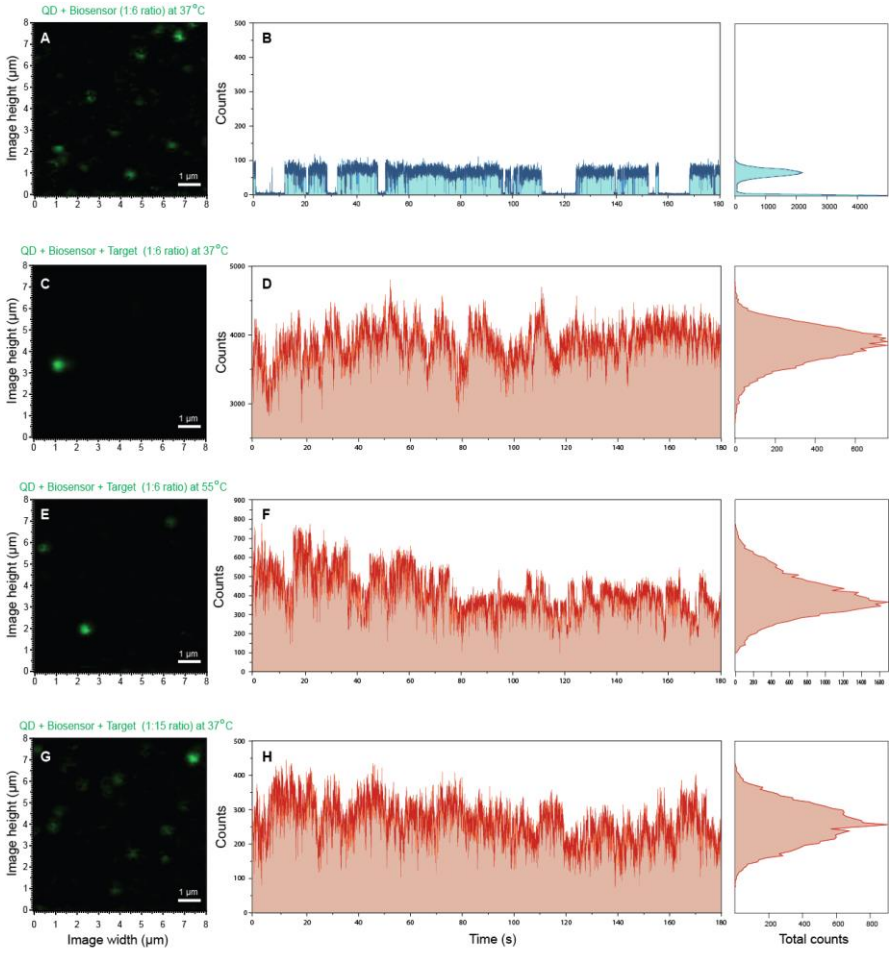

Figure 21: Fluorescence micrograms of images and corresponding blinking trajectories. All the samples were analyzed at a concentration of 800 pM. A-B: QDs + sensor (at 1:6 ratio), C-D: QDs + sensor (1:6) after incubation with target strands at 37 °C, E-F: QDs + sensor (1:6) after incubation with target strands at 55 °C measured, and G-H: QDs + sensor (1:15) after incubation with target strands at 37 °C. *This image was adapted from our publication.*[26]

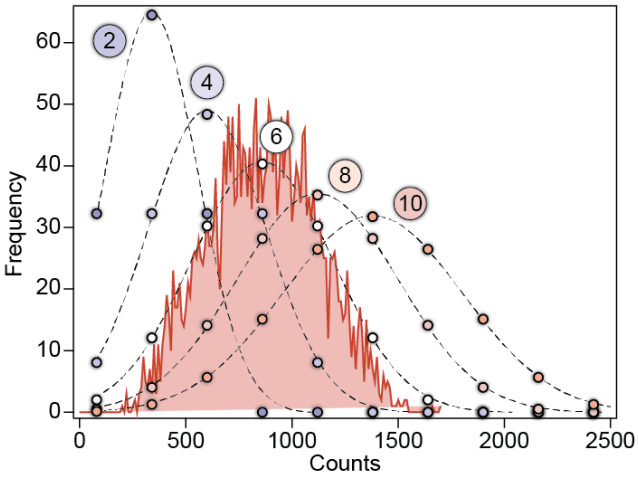

Figure 22: Binomial model was used to plot probability distributions of finding 2-10 QDs in the DNA-QD lattice from the blinking trace and intensity histogram in Figure 20D. *This image was adapted from our publication*.[26]

CHAPTER 4: THERANOSTICS AND FUTURE DIRECTIONS

4.1 Theranostic Probes

Theranostic probes in nanomedicine is described as the simultaneous integration of diagnostic and therapeutic agents in one probe that can be used to treat chronic ailments such as cancers, diabetes mellitus, cardiovascular and neurodegenerative diseases by utilizing various nano-carriers to deliver encapsulated pharmaceuticals coupled with imaging agents.[86-88] The goal of the encapsulations are to diagnose, deliver, and monitor responses in-real time.[87, 88] Imaging mechanisms play a fundamental role in diagnostics such as MRI contrast agents using iron oxide nanoparticles, fluorescence tags or the use the quantum dots (QDs) that have different pay loads to promote specific therapeutic activities for example, folate receptor antagonist.

4.2 RNA Interference (RNAi)

Andrew Fire, Craig Mello, and colleagues discovered the natural cellular response of RNAi by showing that dsRNA induced gene silencing more efficiently than either the sense or antisense RNAs alone.[89, 90] It is valuable to provide a rudimentary explanation of the RNAi pathway. RNAi can be induced by either micro-RNAs and short-interfering RNAs (siRNAs).[91] These two RNAs undergo different processing pathways, but converge once loaded on to the RNA-induced silencing complex.[91] A long, linear, and completely complementary dsRNA, for example Dicer Substrate RNAs that are exogenously introduced into the cell. These dsRNAs are recognized by Dicer which cleaves the target to produce dsRNAs that are 21-25 nts long with 2 nt 3’ overhangs (Figure 23).[91-95]

The siRNAs are introduced to the Argonaute (Ago) family proteins found in humans to generate the RISC (RNA-induced silencing complex) by the association of Dicer, TRBP, and Ago-2, also known as the RISC-loading complex.[91] The complex selects the strand in the miRNA with less thermodynamically stable base-pairing at its 5'-end as the guide strand.[91] Ago 2 is the only protein of the family that exhibits enzymatic slicer activity using perfect complementarity through the guide (antisense) strand to the messenger RNA (mRNA) target site or Ago 1, 3, and 4 inducing translational repression leading to deadenylation of poly A-tail and mRNA degradation, the former is not required for gene silencing[91, 96].

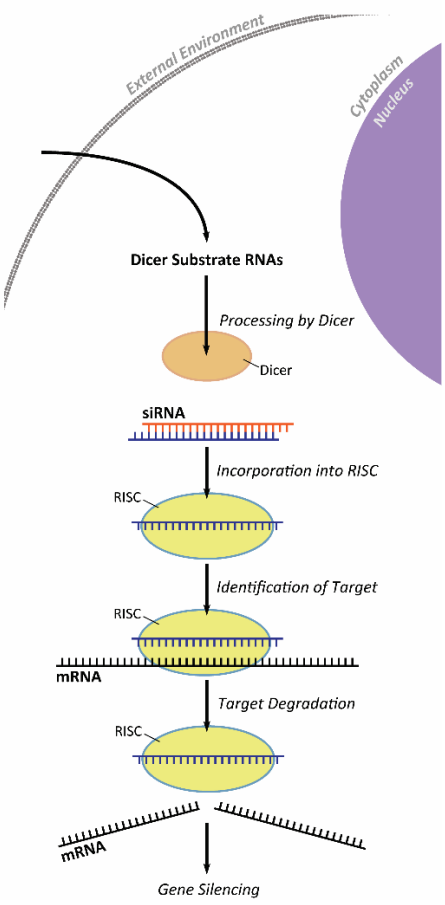

Figure 23: Hijacking of natural cellular gene silencing mechanism by intracellular introduction of Dicer Substrate RNAs and RNA interference (RNAi) *Figure credit: Morgan Chandler*

4.3 Dicer Substrate RNAs and DNA/RNA Hybrid Re-Association and formation of QD lattices

Dicer substrates RNAs (DS RNAs) are slightly longer dsRNAs that are processed by Dicer into siRNAs, before being loaded onto the RISC.[98, 99] Afonin *et al.*[100] designed a split RNA/DNA hybrids that re-associate using a 12 nt ssDNA toehold. The recognition of the complementary sequence causes the release of DS RNAs. Similarly, we have used this same RNA-DNA hybrid concept that contains biotinylated DNAs that are bound to QDs. Upon the interaction of the ssDNAs, form a QD-DNA lattice and releases DS RNAs against enhanced green fluorescent protein (eGFP) that use ssDNA toeholds to cross-link QDs together, thereby releasing the Dicer substrate RNAs.

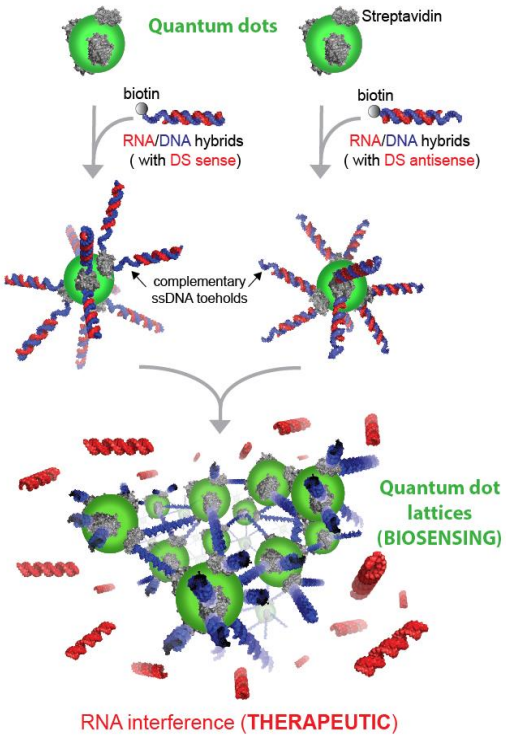

Figure 24: Nucleic acid theranostic probe through the utilization of QDs that are bound to RNA-DNA hybrids that can re-associate upon the interaction with its complementary sequence. This causes a branch migration and the subsequent. *Figure credit Dr. Kirill Afonin*

Transfection experiments were performed with the human breast cancer cell line, MDA-MB-231, with and without GFP. We present the utilization of this concept as the development into a theranostic probe. First, to observe the uptake efficiency QDs bound to each hybrid separately, mixed hybrids, and lattices were transfected using lipofectamine 2000 and quantified by flow cytometry and fluorescence confocal microscopy. The geometric mean fluorescence intensity (gMFI) increased by ~30% when both hybrids were transfected together rather than each hybrid separately. It is important to note that the lattices were not taken up as efficiently into the cells, which resulted in a lower gMFI signal (Figure 26). We decided to use a multiplexed assay using two different sized QDs, QD 545 (green) and QD 605 (red) to determine whether the hybrids co-localize in the same location, which shows reasonable conclusions that the hybrids could re-associate inside the cell (Figure 26).

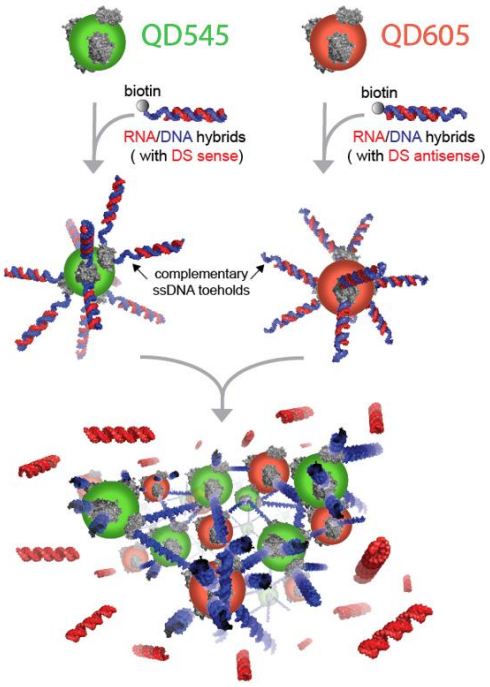

Figure 25: RNA-DNA hybrid co-localization using two different sized quantum dots. *Figure credit: Dr. Kirill Afonin*

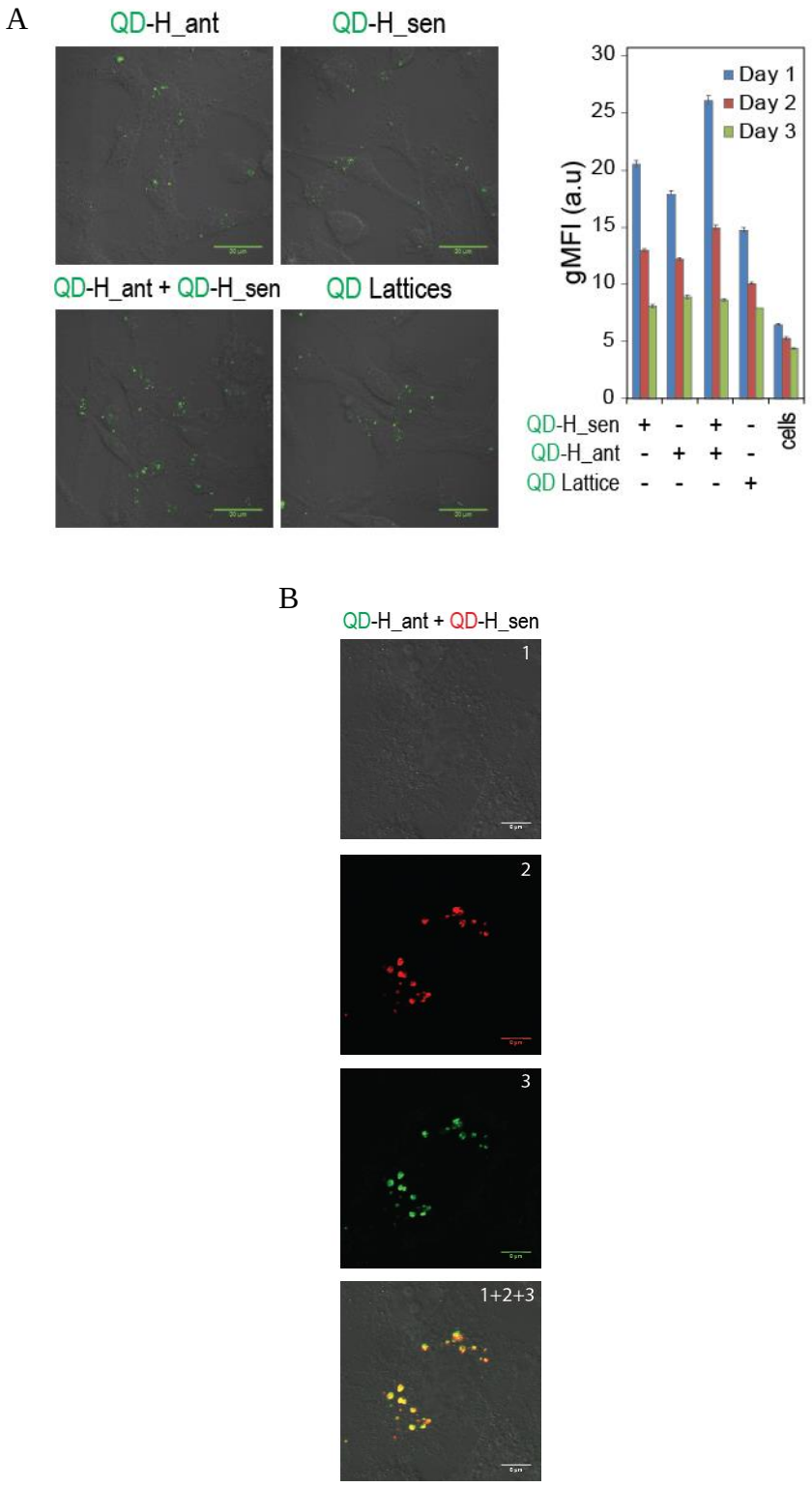

Figure 26: Transfection and co-localization experiments. A. RNA-DNA hybrids were transfected into MDA-MB-231 breast cancer cells. When both hybrids (sense and antisense) were transfected together, the gMFI increased by ~30%. B. Co-localization of two different sized QDs localized in the same location in the cell.

Finally, silencing experiments were performed to confirm the re-association of the hybrids and the release of DS RNAs against enhanced green fluorescent protein (eGFP). In the presence of both hybrids, the gMFI decreased by ~50% when compared to cells alone (Figure 27).

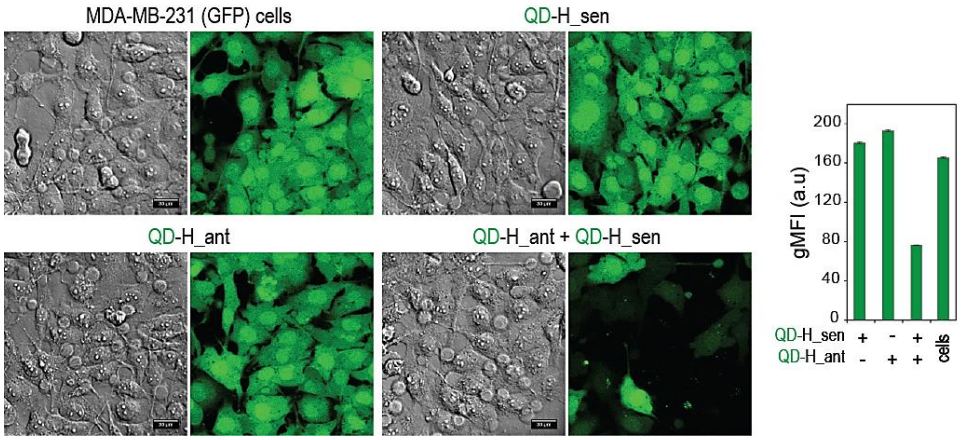

Figure 27: Silencing experiments using DS RNAs release by the re-association of RNA-DNA hybrids caused ~50% silencing efficiency of enhanced green fluorescence protein expressed in MDA-MB-231 breast cancer cell line.

CONCLUSION

Throughout this work, we have provided a unique and versatile approach to biosensing using a nucleic acid biosensor that can undergo a ssDNA strand displacement in the presence of an oncogene target (K-*ras*). This re-association caused the formation of a double biotinylated DNA duplex that can then be cross-linked by QDs. By imaging these DNA-QD assemblies via confocal time-resolved fluorescence microscopy, different Poisson distributions can distinguish between single and aggregated QDs. In future work we hope to expand a library of QD-based lattice assemblies with different length of oligonucleotides, thus forming lattices of different sizes and cross-linking nucleic acid distances. This could show unique properties that can perhaps distinguish between larger and smaller lattice assemblies. Lastly, by combining both a diagnostics (biosensing) and therapeutics (RNAi) we can develop a theranostic device that can be used in a proof of concept to determine the reality of using nucleic acid-QD assemblies as an efficient option for cancer diagnosis and therapy.

REFERENCES

1. Sin, M. L.; Mach, K. E.; Wong, P. K.; Liao, J. C. *Expert review of molecular diagnostics* **2014,** 14, (2), 225-244.

2. Mabey, D.; Peeling, R. W.; Ustianowski, A.; Perkins, M. D. *Nature reviews. Microbiology* **2004,** 2, (3), 231.

3. Mascini, M.; Tombelli, S. *Biomarkers* **2008,** 13, (7-8), 637-657.

4. Bohunicky, B.; Mousa, S. A. *Nanotechnology, science and applications* **2011,** 4, (1), 1-10.

5. Wagner, P. D.; Srivastava, S. *Translational Research* **2012,** 159, (4), 343-353.

6. Perumal, V.; Hashim, U. *Journal of Applied Biomedicine* **2014,** 12, (1), 1-15.

7. Kirsch, J.; Siltanen, C.; Zhou, Q.; Revzin, A.; Simonian, A. *Chemical Society Reviews* **2013,** 42, (22), 8733-8768.

8. Grieshaber, D.; MacKenzie, R.; Voeroes, J.; Reimhult, E. *Sensors* **2008,** 8, (3), 1400-1458.

9. Holzinger, M.; Le Goff, A.; Cosnier, S. *Frontiers in chemistry* **2014,** 2, 63.

10. Thevenot, D. R.; Toth, K.; Durst, R. A.; Wilson, G. S. *Pure and applied chemistry* **1999,** 71, (12), 2333-2348.

11. Morrison, D. W.; Dokmeci, M. R.; Demirci, U.; Khademhosseini, A., *Clinical applications of micro-and nanoscale biosensors*. John Wiley & Sons, Inc.: Hoboken, NJ, USA: 2007.

12. Cunningham, D. D.; Stenken, J. A., *In vivo glucose sensing*. John Wiley & Sons: 2009; Vol. 174.

13. Turner, A. P. *Chemical Society Reviews* **2013,** 42, (8), 3184-3196.

14. Luong, J. H.; Male, K. B.; Glennon, J. D. *Biotechnology advances* **2008,** 26, (5), 492-500.

15. Updike, S.; Hicks, G. *Nature* **1967,** 214, (5092), 986-988.

16. Clemens, A.; Chang, P.; Myers, R. *Hormone and metabolic research= Hormon- und Stoffwechselforschung= Hormones et metabolisme* **1977**, 23.

17. Wang, J. *Chemical reviews* **2008,** 108, (2), 814-825.

18. Liu, Q.; Wang, P., *Cell-based biosensors: principles and applications*. Artech House: 2009.

19. Donahue, A. C.; Albitar, M., Antibodies in biosensing. In *Recognition Receptors in Biosensors*, Springer: 2010; pp 221-248.
20. Bhatta, D.; Stadden, E.; Hashem, E.; Sparrow, I.; Emmerson, G. *Journal of immunological methods* **2010,** 362, (1), 121-126.

21. Du, Y.; Dong, S. *Anal. Chem* **2017,** 89, (1), 189-215.

22. Pedrero, M.; Campuzano, S.; Pingarrón, J. M. *Sensors* **2009,** 9, (7), 5503-5520.

23. Noomnarm, U.; Clegg, R. M. *Photosynth Res Photosynthesis Research : Official Journal of the International Society of Photosynthesis Research* **2009,** 101, (2-3), 181-194.

24. Skoog, D. A.; Holler, F. J.; Crouch, S. R., *Instrumental analysis*. Brooks/Cole, Cengage Learning Belmont: 2007.

25. Albrecht, C. *Anal Bioanal Chem Analytical and Bioanalytical Chemistry* **2008,** 390, (5), 1223-1224.

26. Roark, B.; Tan, J. A.; Ivanina, A.; Chandler, M.; Castaneda, J.; Kim, H. S.; Jawahar, S.; Viard, M.; Talic, S.; Wustholz, K. L. *ACS Sensors* **2016,** 1, (11), 1295-1300.

27. Kramer, D.; Cannon Jr, P.; Guilbault, G. *Analytical Chemistry* **1962,** 34, (7), 842-845.
28. Watson, J. D.; Crick, F. H. *Annals of the New York Academy of Sciences-Paper Edition* **1995,** 758, (12).

29. Egli, M.; Saenger, W., *Principles of nucleic acid structure*. Springer Science & Business Media: 2013.

30. Afonin, K. A.; Kasprzak, W. K.; Bindewald, E.; Kireeva, M.; Viard, M.; Kashlev, M.; Shapiro, B. A. *Accounts Chem Res* **2014,** 47, (6), 1731-41.

31. Afonin, K. A.; Viard, M.; Koyfman, A. Y.; Martins, A. N.; Kasprzak, W. K.; Panigaj, M.; Desai, R.; Santhanam, A.; Grabow, W. W.; Jaeger, L. *Nano letters* **2014,** 14, (10), 5662-5671.

32. Halman, J. R.; Satterwhite, E.; Roark, B.; Chandler, M.; Viard, M.; Ivanina, A.; Bindewald, E.; Kasprzak, W. K.; Panigaj, M.; Bui, M. N.; Lu, J. S.; Miller, J.; Khisamutdinov, E. F.; Shapiro, B. A.; Dobrovolskaia, M. A.; Afonin, K. A. *Nucleic Acids Res* **2017**.

33. Zadeh, J. N.; Steenberg, C. D.; Bois, J. S.; Wolfe, B. R.; Pierce, M. B.; Khan, A. R.; Dirks, R. M.; Pierce, N. A. *Journal of computational chemistry* **2011,** 32, (1), 170-173.

34. Feng, S.; Shang, Y.; Wu, F.; Ding, F.; Li, B.; Xu, J.; Xu, L.; Zhou, X. *Talanta* **2014,** 120, 141-147.

35. Zhou, J.; Rossi, J. *Nat Rev Drug Discov* **2017,** 16, (3), 181-202.

36. Weinberg, M. S. *Mol Ther Nucleic Acids* **2014,** 3, e194.

37. Ellington, A. D.; Szostak, J. W. *nature* **1990,** 346, (6287), 818.

38. Keefe, A. D.; Cload, S. T. *Current Opinion in Chemical Biology* **2008,** 12, (4), 448-456.

39. Shamah, S. M.; Healy, J. M.; Cload, S. T. *Accounts Chem Res* **2008,** 41, (1), 130-138.

40. Cagnin, S.; Caraballo, M.; Guiducci, C.; Martini, P.; Ross, M.; SantaAna, M.; Danley, D.; West, T.; Lanfranchi, G. *Sensors* **2009,** 9, (4), 3122-3148.

41. Cho, H.; Yeh, E.-C.; Sinha, R.; Laurence, T. A.; Bearinger, J. P.; Lee, L. P. *ACS nano* **2012,** 6, (9), 7607-7614.

42. Ren, J.; Wang, T.; Wang, E.; Wang, J. *Analyst* **2015,** 140, (8), 2556-2572.

43. Chen, Q.; Zuo, J.; Chen, J.; Tong, P.; Mo, X.; Zhang, L.; Li, J. *Biosensors and Bioelectronics* **2015,** 72, 326-331.

44. Chua, A.; Yean, C. Y.; Ravichandran, M.; Lim, B.; Lalitha, P. *Biosensors and Bioelectronics* **2011,** 26, (9), 3825-3831.

45. Yang, L.; Tao, Y.; Yue, G.; Li, R.; Qiu, B.; Guo, L.; Lin, Z.; Yang, H. H. *Analytical chemistry* **2016,** 88, (10), 5097-103.

46. Lan, J.; Liu, Y.; Li, L.; Wen, F.; Wu, F.; Han, Z.; Sun, W.; Li, C.; Chen, J. *Scientific reports* **2016,** 6.

47. Liu, A.; Wang, K.; Weng, S.; Lei, Y.; Lin, L.; Chen, W.; Lin, X.; Chen, Y. *TRAC Trends in Analytical Chemistry* **2012,** 37, 101-111.

48. Xuan, F.; Luo, X.; Hsing, I. M. *BIOS Biosensors and Bioelectronics* **2012,** 35, (1), 230-234.

49. Du, Y.; Lim, B. J.; Li, B.; Jiang, Y. S.; Sessler, J. L.; Ellington, A. D. *Analytical chemistry* **2014,** 86, (15), 8010-6.

50. Smith, A. M.; Nie, S. *Accounts Chem Res* **2009,** 43, (2), 190-200.

51. Brus, L. E. *The Journal of chemical physics* **1984,** 80, (9), 4403-4409.

52. Alivisatos, A. P. *The Journal of Physical Chemistry* **1996,** 100, (31), 13226-13239.

53. Zhou, J.; Yang, Y.; Zhang, C.-y. *Chemical reviews* **2015,** 115, (21), 11669-11717.

54. Jin, Z.; Hildebrandt, N. *Trends Biotechnol.* **2012,** 30, (7), 394-403.

55. Kairdolf, B. A.; Smith, A. M.; Stokes, T. H.; Wang, M. D.; Young, A. N.; Nie, S. *Annual Review of Analytical Chemistry* **2013,** 6, 143-162.

56. Michalet, X.; Pinaud, F.; Bentolila, L.; Tsay, J.; Doose, S.; Li, J.; Sundaresan, G.; Wu, A.; Gambhir, S.; Weiss, S. *science* **2005,** 307, (5709), 538-544.

57. Goldman, E. R.; Balighian, E. D.; Mattoussi, H.; Kuno, M. K.; Mauro, J. M.; Tran, P. T.; Anderson, G. P. *Journal of the American Chemical Society* **2002,** 124, (22), 6378-6382.

58. Cordones, A. A.; Leone, S. R. *Chemical Society Reviews* **2013,** 42, (8), 3209-3221.

59. Zhou, H.; Liu, J.; Zhang, S. *TRAC Trends in Analytical Chemistry* **2015,** 67, 56-73.

60. Chakravarthy, K. V.; Davidson, B. A.; Helinski, J. D.; Ding, H.; Law, W.-C.; Yong, K.-T.; Prasad, P. N.; Knight, P. R. *Nanomedicine: Nanotechnology, Biology and Medicine* **2011,** 7, (1), 88-96.

61. El-Sayed, M. A. *Accounts Chem Res* **2004,** 37, (5), 326-33.

62. Medintz, I. L.; Uyeda, H. T.; Goldman, E. R.; Mattoussi, H. *Nature materials* **2005,** 4, (6), 435-446.

63. Chan, W. C.; Maxwell, D. J.; Gao, X.; Bailey, R. E.; Han, M.; Nie, S. *Curr. Opin. Biotechnol.* **2002,** 13, (1), 40-46.

64. Han, M.; Gao, X.; Su, J. Z.; Nie, S. *Nature biotechnology* **2001,** 19, (7), 631-635.

65. Frasco, M. F.; Chaniotakis, N. *Sensors (Basel)* **2009,** 9, (9), 7266-86.

66. Jaiswal, J. K.; Goldman, E. R.; Mattoussi, H.; Simon, S. M. *Nat Biotech* **2003,** 21.
67. Jiang, H.; Wang, X. *Analytical chemistry* **2012,** 84, (16), 6986-93.

68. Silvi, S.; Credi, A. *Chemical Society Reviews* **2015,** 44, (13), 4275-4289.

69. Bahshi, L.; Freeman, R.; Gill, R.; Willner, I. *Small* **2009,** 5, (6), 676-680.

70. Oh, S.-D.; Duong, H. D.; Rhee, J. I. *YABIO Analytical Biochemistry* **2015,** 483, 54-61.

71. Medintz, I. L.; Clapp, A. R.; Brunel, F. M.; Tiefenbrunn, T.; Uyeda, H. T.; Chang, E. L.; Deschamps, J. R.; Dawson, P. E.; Mattoussi, H. *Nature materials* **2006,** 5, (7), 581.

72. Xia, Z.; Xing, Y.; So, M.-K.; Koh, A. L.; Sinclair, R.; Rao, J. *Analytical chemistry* **2008,** 80, (22), 8649-8655.
73. Zhu, J.-J.; Li, J.-J.; Huang, H.-P.; Cheng, F.-F., *Quantum dots for DNA biosensing*. Springer: 2013.
74. Tyagi, S.; Kramer, F. R. *Nature biotechnology* **1996,** 14, (3), 303-8.

75. Smith, A. M.; Nie, S. *Accounts Chem Res* **2010,** 43, (2), 190-200.

76. Krauss, T. D.; Peterson, J. J. *The Journal of Physical Chemistry Letters* **2010,** 1, (9), 1377-1382.

77. Nirmal, M.; Dabbousi, B. O.; Bawendi, M. G.; Macklin, J. *Nature* **1996,** 383, (6603), 802.

78. Empedocles, S. A.; Norris, D.; Bawendi, M. *Physical review letters* **1996,** 77, (18), 3873.
79. Schwartz, O.; Oron, D. *Israel Journal of Chemistry* **2012,** 52, (11-12), 992-1001.

80. Rosen, S.; Schwartz, O.; Oron, D. *Physical review letters* **2010,** 104, (15), 157404.

81. Darby, R. A.; Sollogoub, M.; McKeen, C.; Brown, L.; Risitano, A.; Brown, N.; Barton, C.; Brown, T.; Fox, K. R. *Nucleic Acids Research* **2002,** 30, (9), e39-e39.

82. Makovets, S. **2013**.

83. Víglaský, V.; Antalík, M.; Bagel'ová, J.; Tomori, Z.; Podhradský, D. *Electrophoresis* **2000,** 21, (5), 850-858.

84. Binzel, D. W.; Khisamutdinov, E. F.; Guo, P. *Biochemistry* **2014,** 53, (14), 2221-2231.

85. Dragan, A.; Pavlovic, R.; McGivney, J.; Casas-Finet, J.; Bishop, E.; Strouse, R.; Schenerman, M.; Geddes, C. *Journal of fluorescence* **2012,** 22, (4), 1189-1199.

86. Muthu, M. S.; Leong, D. T.; Mei, L.; Feng, S.-S. *Theranostics* **2014,** 4, (6), 660-677.

87. Ahmed, N.; Fessi, H.; Elaissari, A. *Drug discovery today* **2012,** 17, (17), 928-934.

88. Lammers, T.; Aime, S.; Hennink, W. E.; Storm, G.; Kiessling, F. *Accounts of chemical research* **2011,** 44, (10), 1029-1038.

89. Fire, A.; Xu, S.; Montgomery, M. K.; Kostas, S. A.; Driver, S. E.; Mello, C. C. *nature* **1998,** 391, (6669), 806-811.

90. Liu, H.; Li, Y.; Mozhi, A.; Zhang, L.; Liu, Y.; Xu, X.; Xing, J.; Liang, X.; Ma, G.; Yang, J. *Biomaterials* **2014,** 35, (24), 6519-6533.

91. Wilson, R. C.; Doudna, J. A., Molecular Mechanisms of RNA Interference. In *Annual Review of Biophysics, Vol 42*, Dill, K. A., Ed. 2013; Vol. 42, pp 217-239.

92. Saini, H. K.; Griffiths-Jones, S.; Enright, A. J. *Proceedings of the National Academy of Sciences* **2007,** 104, (45), 17719-17724.

93. Kim, Y.-K.; Kim, V. N. *EMBO Journal* **2007,** 26, (3).

94. Lund, E.; Dahlberg, J. In *Substrate selectivity of exportin 5 and Dicer in the biogenesis of microRNAs*, Cold Spring Harbor symposia on quantitative biology, 2006; Cold Spring Harbor Laboratory Press: pp 59-66.

95. Carthew, R. W.; Sontheimer, E. J. *Cell* **2009,** 136, (4), 642-55.

96. Jackson, R. J.; Standart, N. *Sci Stke* **2007,** 367, (re1).

97. Halman, J. R.; Satterwhite, E.; Roark, B.; Chandler, M.; Viard, M.; Ivanina, A.; Bindewald, E.; Kasprzak, W. K.; Panigaj, M.; Bui, M. N. *Nucleic Acids Research* **2017,** 45, (4), 2210-2220.

98. Rose, S. D.; Kim, D.-H.; Amarzguioui, M.; Heidel, J. D.; Collingwood, M. A.; Davis, M. E.; Rossi, J. J.; Behlke, M. A. *Nucleic acids research* **2005,** 33, (13), 4140-4156.

99. Kim, D. H.; Behlke, M. A.; Rose, S. D.; Chang, M. S.; Choi, S.; Rossi, J. J. *Nature biotechnology* **2005,** 23, (2), 222-6.

100. Afonin, K. A.; Viard, M.; Martins, A. N.; Lockett, S. J.; Maciag, A. E.; Freed, E. O.; Heldman, E.; Jaeger, L.; Blumenthal, R.; Shapiro, B. A. *Nature nanotechnology* **2013,** 8, (4), 296-304.